Emergency Response Measures to Alleviate a Severe Haze Pollution Event in Northern China during December 2015: Assessment of Effectiveness

Yaping Ma[1], Tzung-May Fu[2,3]*, Heng Tian[1], Jian Gao[4], Min Hu[5], Jianping Guo[6], Yangmei Zhang[7], Yele Sun[8], Lijuan Zhang[1], Xin Yang[2,3], Xiaofei Wang[9,10]

[1] Department of Atmospheric and Oceanic Sciences, Peking University, Beijing 100871, China

[2] State Environmental Protection Key Laboratory of Integrated Surface Water-Groundwater Pollution Control, School of Environmental Science and Engineering, Southern University of Science and Technology, Guangdong 518055, China

[3] Shenzhen Institute of Sustainable Development, Southern University of Science and Technology, Guangdong 518055, China

[4] State Key Laboratory of Environmental Criteria and Risk Assessment, Chinese Research Academy of Environmental Science, Beijing 100012, China

[5] State Key Joint Laboratory of Environmental Simulation and Pollution Control, College of Environmental Sciences and Engineering, Peking University, Beijing 100871, China

[6] State Key Laboratory of Severe Weather, Chinese Academy of Meteorological Sciences, Beijing 100081, China

[7] Key Laboratory of Atmospheric Chemistry, Chinese Academy of Meteorological Sciences, Beijing 100081, China

[8] State Key Laboratory of Atmospheric Boundary Layer Physics and Atmospheric Chemistry, Institute of Atmospheric Physics, Chinese Academy of Sciences, Beijing 100191, China

[9] Shanghai Key Laboratory of Atmospheric Particle Pollution and Prevention, Department of Environmental Science and Engineering, Fudan University, Shanghai 200433, China

[10] Shanghai Institute of Pollution Control and Ecological Security, Shanghai 200092, China

*Correspondence to: fuzm@sustech.edu.cn

Abstract

We used the WRF-Chem model to simulate the surface $PM_{2.5}$ concentrations over the Northern China Plain (NCP) during a severe haze event between December 6 and 10, 2015, with the goal of assessing the effectiveness of the emergency response measures (ERMs) implemented during this period to alleviate the haze pollution. We estimated that, with the exception of NH_3, anthropogenic pollutant emissions were significantly reduced by 8% to 48% over the NCP during December 6 to 10 as a result of the ERM-implementation. Our simulations using the reduced anthropogenic emissions reproduced the observed $PM_{2.5}$ concentrations and compositions over the NCP during the severe haze event. During the haze event, stagnant regional meteorological conditions led to a lengthening of the $PM_{2.5}$ lifetime in the NCP boundary layer to 5 days, compared to a 1-day lifetime during the preceeding clean period. During the severe haze event, only approximately 20% of the surface $PM_{2.5}$ in Beijing was attributable to local emissions, while more than 62% of the surface $PM_{2.5}$ in the rest of NCP was attributable to local emissions. We found that the effects of the implemented ERMs to be modest, reducing the mean surface $PM_{2.5}$ concentrations during the polluted period by 7% in Beijing and by 4% for the rest of the NCP. This modest effect was because the duration of the ERM enforcement was much shorter than the lifetime of $PM_{2.5}$ during the haze event, such that there was insufficient time for the $PM_{2.5}$ concentrations to fully reflect the reduction in emissions. We conclude that anthropogenic emissions in the NCP during severe wintertime haze events would have to be reduced by a much larger percentage if more pronounced abatement of $PM_{2.5}$ concentrations were desired.

Keywords:

$PM_{2.5}$; Severe haze; Emission reduction; Northern China; WRF-Chem.

1. Introduction

The Northern China Plain region (hereafter referred to as the NCP, as shown in Fig 1b), including the Beijing-Tianjin-Hebei (BTH) area and the surrounding provinces of Shandong and Henan, has been experiencing severe winter haze pollution events of hourly $PM_{2.5}$ concentrations exceeding 150 μg m^{-3} in recent years (Dang and Liao, 2019), which pose threats to public health (e.g., Chen et al., 2013). These severe wintertime $PM_{2.5}$ pollution events are typically associated with the accumulation of $PM_{2.5}$ and its precursors under stagnant weather conditions. Such stagnant conditions prevent the horizontal and vertical ventilation of pollutants and are often associated high humidity near the surface, which in turn promotes secondary $PM_{2.5}$ production (Jeong and Park 2013; R. Zhang et al., 2014; Tie et al., 2017; Leung et al., 2018; Zhang et al., 2018). The NCP is blocked by mountains to the north and to the west, which also contributes to the accumulation of $PM_{2.5}$ and its precursors under calm or southerly wind conditions (F. Wang et al., 2010; Wang et al., 2019). These severe winter haze events are terminated by the passage of a cold front, which ventilates the region with strong wind and clean air from the north (J. Wang et al., 2017).

In September 2013, the State Council of China promulgated the "Air Pollution Prevention and Control Action Plan" (State Council of the People's Republic of China, 2013; hereafter referred to as the "Action Plan"), which outlined the policies on reducing nationwide anthropogenic emissions, as well as set specific improvement targets for the annual mean $PM_{2.5}$ concentrations for key areas, including Beijing and the BTH area, by 2017. Between 2013 and 2018, the annual mean $PM_{2.5}$ concentrations for most Chinese cities have dropped (Ministry of Environmental Protection of the People's Republic of China, 2014, 2015, 2016, 2017; Ministry of Ecology and Environment of the People's Republic of China, 2018, 2019), likely in part due to the nationwide emission reduction. The annual mean $PM_{2.5}$ concentrations in Beijing and in BTH in 2017 were reduced to 58 μg m^{-3} and 64 μg m^{-3} (Ministry of Ecology and Environment of the People's Republic of China, 2018), respectively, both meeting the improvement targets set by the "Action Plan". However, analyses of observations showed that the frequency and intensity of wintertime haze events over the NCP have not shown significant decline since 2013 (Q. Zhang et al., 2018; Dang and Liao, 2019).

To alleviate the severe haze events, the "Action Plan" mandated that local Environmental Protection Bureaus and Meteorological Bureaus join forces to establish a protocol for the issuance

and execution of emergency response measures (ERMs). For the NCP area, "Monitoring and Warning Scheme for Heavy Pollution Weather in Beijing, Tianjin, Hebei, and Its Surrounding Areas" was issued in September 2013 to combat severe haze events (Ministry of Environmental Protection of the People's Republic of China, 2013). This scheme categorized the severity of local air pollution into four levels, based on the duration for which the forecasted hourly Air Quality Index (AQI) exceeds 200 (equivalent to hourly $PM_{2.5}$ exceeding 150 μg m^{-3}). When such severe $PM_{2.5}$ pollution events are forecasted, the provincial and municipal governments are to issue emergency alerts at least 24 hours in advance. Each alert level corresponds to a set of ERMs to reduce anthropogenic pollutant emissions (Table S1):

(1) Blue alert: hourly $PM_{2.5}$ concentrations are forecasted to exceed 150 μg m^{-3} and to persist for 24 hours.

(2) Yellow alert: hourly $PM_{2.5}$ concentrations are forecasted to exceed 150 μg m^{-3} and to persist for 48 hours.

(3) Orange alert: hourly $PM_{2.5}$ concentrations are forecasted to exceed 150 μg m^{-3} and to persist for 72 hours.

(4) Red alert: hourly $PM_{2.5}$ concentrations are forecasted to exceed 150 μg m^{-3} and to persist for more than 72 hours.

On December 5, 2015, at 11:00 UTC (19:00 local time), the Beijing municipal government issued an orange alert for severe haze pollution, with the corresponding ERMs to be initiated at 16:00 UTC of December 6. The City of Tianjin and most cities in Hebei, Henan, and Shandong provinces issued various alert levels for severe haze pollution, with corresponding ERMs to be initiated between 16:00 UTC of December 5 and 16:00 UTC of December 7 (Fig. S1). The City of Beijing later upgraded its alert level to the first-ever red alert at 10:00 UTC December 7, with the corresponding stricter ERMs to be initiated at 23:00 UTC December 7. Tianjin and Hebei also updated their alert levels, with stricter ERMs to be initiated between 23:00 UTC December 7 to 16:00 UTC December 8 (Fig. S1). The issuance of the red alert led to the enforcement of stricter emission reduction measures, including the emergency shut-down of more industrial plants and further restrictions of vehicle numbers on the road (Table S1). This was the first time the Chinese

government evoked restrictive ERMs based on air quality forecasts to mitigate severe pollution events. Though the alert levels issued in the NCP varied, the ERM-initiation times in > 90% of the cities were within 16 hours of the ERM-initiation times in Beijing. We referred to the emission reductions in two stages according to the ERM-initiation times in Beijing (Fig S1). Stage I was between 16:00 UTC of December 6 and 23:00 UTC of December 7, during which the orange alert was in effect in Beijing and Henan, and the yellow alert was in effect in Tianjin, Hebei, and Shandong. Stage II was between 23:00 UTC of December 7 and 04:00 UTC of December 10, during which the red alert was in effect in Beijing, the orange alert was in effect in Tianjin, Hebei, and Henan, and the yellow alert was in effect in Shandong.

The Chinese government had previously administered pre-planned emission controls before and during several important events that took place in Beijing to improve the local air quality (Table S2). Such events included the Sino-African Summit in November 2006 (Wang et al., 2007; Cheng et al., 2008), the Beijing Olympic Games in August 2008 (S. Wang et al., 2010; Schleicher et al., 2012), the Asia-Pacific Economy Cooperation (APEC) Summit in November 2014 (Li et al., 2015; Guo et al., 2016a; Zhang et al., 2016; H. Liu et al., 2017), and the Chinese Military Parade in September 2015 (G. Wang et al., 2017; Huang et al., 2018). The emission control actions taken included temporary closures of factories, restrictions on the numbers and types of on-road motor vehicles, and restrictions on constructions. The control actions were enforced in Beijing and its surrounding cities and provinces, including Tianjin, Hebei, Shandong, Shanxi, Henan and the Inner Mongolia Autonomous Region. The resulting reductions in primary pollutant emissions were estimated to be 40% to 70% in Beijing and 30% to 70% in the surrounding cities and provinces (Wang et al., 2007; Liu et al., 2015). Previous studies estimated that these emission control actions may have led to dramatic declines in SO_2, NO_x, and $PM_{2.5}$ concentrations in Beijing and its surrounding areas by 30% to 70% during the APEC (Liu et al., 2015; Zhang et al., 2016) and by 50% during the Chinese Military Parade (G. Wang et al., 2017). However, these pre-planned emission controls were enforced over much larger spatial areas, often lasted for weeks, and were in most cases stricter than the ERMs implemented during December 6-10, 2015. More importantly, those previous events all took place either in summer or in fall, when the regional meteorological conditions were more favorable to the dispersion or removal of pollutants, aiding the efficacy of the

emission control actions (Zhang et al., 2016; Huang et al., 2018).

In comparison, the short-term ERMs administered during severe wintertime haze events were likely to be less effective, because the stagnant meteorological conditions impeded pollutant dispersion, the controls were less strict, and the enforcement was over a smaller domain and for a shorter period of time. A few studies have attempted to quantify the impacts of emission reduction measures on the $PM_{2.5}$ concentrations in the NCP during haze events or haze seasons, but these studies did not distinguish the impacts of China-wide long-term emission controls and the short-term ERMs. Wu et al. (2017) simulated the effects of a hypothetical 30% reduction of monthly anthropogenic emissions in the BTH area during the entire January 2012 and found a 20% decline in the local monthly mean $PM_{2.5}$ concentration. T. Liu et al. (2017) estimated that the overall reduction of anthropogenic emissions since the year 2014 over the NCP led to a 9% decline in the monthly mean $PM_{2.5}$ concentration over the NCP in December 2015 relative to December 2014. Chen et al. (2019) simulated the $PM_{2.5}$ concentrations in Beijing during four seasonal haze episodes (November 2016 versus November 2017; March 2013 versus March 2018). They estimated that the overall reduction of anthropogenic emissions since 2013 led to 33% and 16% decreases of the simulated monthly mean $PM_{2.5}$ concentrations in Beijing in November 2017 and March 2018, relative to November 2016 and March 2013, respectively. However, it is likely that the decline in monthly mean $PM_{2.5}$ concentrations inferred by these three previous studies were mainly due to the long-term emission control in China and not specifically to the ERMs. Wang et al. (2020) hypothetically simulated the effects of emergency emission reduction on $PM_{2.5}$ concentrations during a 5-day severe haze event over the Yangtze River Delta area. They found that a short-term, 20% to 90% reduction of power, transportation, and industry emissions, comparable to the strictest ERMs, would only lead to a 16% reduction in $PM_{2.5}$ concentration. To the best of our knowledge, the effectiveness of the ERMs administered over the NCP area during severe haze events have not been explicitly evaluated.

It is also important to quantitatively assess the relative contributions of local and regional pollutant emissions to the local $PM_{2.5}$ concentrations during severe haze events, in order to help municipal policy-makers formulate effective emergency responses. Zhang et al. (2015) previously found that 50% of the $PM_{2.5}$ in Beijing during January 2013 was due to emissions within Beijing,

while the remaining 50% were due to emissions nearby provinces in Northern China. However, in view of the large emissions reductions in all provinces and cities in Northern China since 2013, that fraction may have changed significantly and should be reevaluated.

In this study, we explicitly simulated surface $PM_{2.5}$ concentrations over the NCP during December 2 to 10, 2015 both with and without the emission reductions associated with the ERMs, to assess the effectiveness of the ERMs on alleviating severe haze pollution. We also quantified the relative contributions of local and regional emissions to $PM_{2.5}$ concentrations in Beijing and over the rest of NCP during this severe haze event. Finally, we analytically interpret the effectiveness/ineffectiveness of the ERMs during this haze event, in order to better inform future emergency response strategies.

2. Model and data

2.1 WRF-Chem model

We used the WRF-Chem regional air quality model version 3.6.1 (Grell et al., 2005) to simulate surface $PM_{2.5}$ over the NCP from November 26 to December 10, 2015. The first 6 days spun up the model; results for December 2 to 10, 2015 were analyzed. Fig 1 shows the two nested domains in our simulations with horizontal resolutions of 81 km and 27 km, respectively. The 27-km horizontal resolution in the inner domain was consistent with the 0.25^{o} resolution of the anthropogenic emission inventory (Section 2.2). The model consisted of 30 vertical layers extending from the surface to 50 hPa, with 7 layers in the bottom 1 km. Meteorological initial and boundary conditions into WRF-Chem were from the NCEP FNL Operational Global Analysis data (Kalnay et al., 1996) and updated every 6 hours. Chemical initial and boundary conditions were from a MOZART global model simulation (Emmons et al., 2010), except we reduced the boundary conditions of dust concentrations by 50% following Georgiou et al. (2018). We nudged the temperature, humidity, and wind in WRF-Chem with hourly surface meteorological measurements and twice-daily rawinsonde profiles over China (Guo et al., 2016b) using four-dimensional data assimilation to reduce errors in the simulated meteorology (Gilliam et al., 2012).

Gas-phase chemistry in WRF-Chem was simulated using the SAPRC-99 mechanism (Carter,

2000), updated to include the photochemistry of dicarbonyls (Li et al., 2013). $PM_{2.5}$ in our model included primary elemental carbon aerosols (EC), primary organic aerosols (POA), secondary inorganic aerosols (sulfate, nitrate, and ammonium), secondary organic aerosols (SOA), anthropogenic and natural dust, and sea salt. Aerosol microphysics and gas-particle partitioning were simulated using the MOSAIC module (Zaveri et al., 2008). SOA productions from anthropogenic and biogenic volatile organic precursors were simulated with the VBS module (Lane et al., 2008). We also included the aqueous uptake of glyoxal and methylglyoxal as a source of SOA (Fu et al., 2008, 2009; Li et al., 2013). We optimized the deposition velocity of fog droplets in WRF-Chem to 0.3 cm s^{-1} to be consistent with the observed fog droplet radius of 2 to 3 μm over the NCP (J. Zhang et al., 2014; Seinfeld and Pandis, 2006).

A number of studies have proposed fast, heterogeneous sulfate production pathways, potentially catalyzed by nitrogen dioxide or metal ions, during severe haze events over the NCP (He et al., 2014; Cheng et al., 2016; Wang et al., 2016; M. Liu et al., 2017; Zhao et al., 2017; Hung et al., 2018; Shao et al., 2019). The exact pathway responsible for the high sulfate concentrations during the severe wintertime haze events in the NCP is still uncertain. Nevertheless, we added in our WRF-Chem simulation the sulfate production via the heterogeneous uptake of SO_2 by aqueous aerosols as parameterized by Wang et al. (2016), on the account that this parameterization led to a good simulation of the observed sulfate concentration during our study period (Section 3.1.2). The production rate of sulfate by the heterogeneous oxidation of SO_2 on particles was parameterized as:

$$\frac{d[\mathrm{SO_4^{2-}}]}{dt}|_{\mathrm{hetero}} = \frac{1}{4}\gamma\bar{v}S_c[\mathrm{SO_2}] \qquad \text{Eq. (1)}$$

$d[SO_4^{2-}]/dt|_{hetero}$ was the rate of heterogeneous production of sulfate (ppmv s^{-1}); γ was the effective uptake coefficient of SO_2 on aqueous aerosol surfaces; $\bar{v}$ was the mean molecular speed of SO_2 (m s^{-1}); S_c was the aerosol surface area density (m^2 m^{-3} dry air); $[SO_2]$ was the gaseous SO_2 concentrations (ppmv). We used the values $\gamma = 1.6 \times 10^{-5}$ for relative humidity (RH) < 41%, $\gamma = 2.1 \times 10^{-5}$ for RH between 41% and 56%, and $\gamma = 4.5 \times 10^{-5}$ for RH > 56%, as observationally constrained by Wang et al. (2016).

2.2 Emissions

Chinese monthly anthropogenic emissions of $PM_{2.5}$ precursors and primary $PM_{2.5}$ were from the Multi-resolution Emission Inventory for China (MEIC), developed by Tsinghua University (http://meicmodel.org, Li et al., 2017) for the year 2016 at a horizontal resolution of 0.25°. Anthropogenic source activities included power generation, industries, residential activities, on-road transportation, and agriculture. Activity levels were based on provincial statistics for the year 2016. Anthropogenic emissions for the rest of Asia were from the MIX inventory (Li et al., 2017), developed for the year 2010 at a horizontal resolution of 0.25°. We applied diurnal variations to transportation and residential emissions (Li et al., 2013). Emissions from power generation were injected into the second vertical layer in the model, approximately 100 m above the surface.

Daily biomass burning emissions were taken from the Fire INventory from NCAR (FINN, version 1.5, Wiedinmyer et al., 2011) for the study period. Dust emissions were calculated online using the Goddard Global Ozone Chemistry Aerosol Radiation and Transport (GOCART) dust scheme (Ginoux et al., 2001) with the Air Force Weather Agency modifications (GOCART-AFWA, LeGrand et al., 2019). Biogenic emissions were calculated online using the MEGAN module (version 2.04, Guenther et al., 2006).

2.3 Emission reductions associated with ERMs

We systematically surveyed the government announcements and news reports released during December 6 to 10, 2015 to determine the issued alert levels, the ERMs administered for each of the cities and provinces in the NCP, and the start/end times of ERM implementation (Table S1, Fig S1). The emission reductions associated with the ERMs for the industrial, residential, and transportation sectors were estimated based on the guidelines and activity advisories in the "Emergency Plan for Heavy Air Pollution" issued by each city or province. Table 1 summarized the percentages of sectoral emission reductions as a result of the ERMs for Beijing, Tianjin, Hebei, Henan, and Shandong, respectively, from December 6 to 10, 2015.

Table 2 shows the calculated short-term reductions in anthropogenic pollutant emissions for each of the cities and provinces in the NCP from December 6 to 10, 2015 using the percentages in Table 1. As shown in Table 2, anthropogenic emissions were reduced most dramatically in Beijing,

due to the enforcement of the strictest ERMs. Anthropogenic emissions of VOCs, SO_2, and NO_x in Beijing during Stage II were reduced by 48%, 34%, and 38%, respectively. Anthropogenic emissions of primary $PM_{2.5}$ constituents, such as EC, POA, and anthropogenic dust, were also significantly reduced in Beijing due to enforced restrictions on residential emissions and constructions. Emissions of most anthropogenic pollutants in Tianjin, Hebei, and Henan were significantly reduced by 11% to 27%, but the emission reductions in Shandong were generally less than 10%. Anthropogenic NH_3 emissions were reduced by only 1% to 9% across the NCP, as NH_3 was mostly emitted by agricultural activities and minimally affected by the ERMs.

Several previous studies have assessed the emission reductions associated with pre-planned emission control actions in Beijing using inverse modeling of observations. For example, satellite-based NO_2 observations indicated that the prohibition of heavy-duty diesel vehicles and the 50%-reduction of vehicle numbers on city roads throughout the NCP reduced the NO_x emission by 30% to 47% in the NCP during the Beijing Olympic Games (S. Wang et al., 2010), the APEC (Huang et al. 2015), and the Chinese Military Parade (Zhang et al. 2017). Similarly, satellite-based SO_2 observations indicated that the reduction of industrial production, the temporary closure of power plants, and the prohibition of heavy-duty diesel vehicles on roads reduced the SO_2 emissions in Beijing by 34% to 46% during the APEC and the Chinese Military Parade (G. Wang et al. 2017, Zhang et al. 2017). These control actions were similar to the ERMs implemented in Beijing during our haze event, and we also estimated a 38% reduction of NO_x emissions and 34% reduction of SO_2 emission in Beijing.

2.4 Measurements of meteorological conditions and air pollutants

Hourly air pollutant concentrations were measured at 239 surface sites across the NCP, operated by the China National Environmental Monitoring Centre (http://www.cnemc.cn). At each site, $PM_{2.5}$ mass concentrations were measured using either the micro-oscillating balance method or the β-absorption method (Ministry of Environmental Protection of the People's Republic of China, 2012).

Hourly $PM_{2.5}$ concentrations were also continuously measured at the Chinese Research

Academy of Environmental Sciences in Beijing (CRAES; 40.04° N, 116.42° E) from December 2 to 10, 2015. The CRAES site is located 8 m above ground in a mixed residential/commercial area with no strong point sources nearby (Gao et al., 2016). Approximately 10 km away, daily 24-h filter samples of $PM_{2.5}$ were collected at the Peking University Urban atmosphere Environment monitoRing Station (PKUERS; 39.99° N, 116.31° E), located on the roof of an academic building (Tang et al., 2018). Teflon filter samples were analyzed for inorganic ions using the DIONEX ICS-2500 and ICS-2000. Quartz filter samples were analyzed for EC and organic carbon (OC) using a thermal-optical instrument (Model-4, Sunset Laboratory) following the NIOSH protocol (Tang et al., 2018).

Meteorological observations used to validate our simulations included hourly measurements at surface weather sites across China, as well as twice-daily rawinsondes in Beijing (39.93° N, 116.28° E), Zhangqiu (36.70° N, 117.55° E; Shandong Province), Taiyuan (37.78° N, 112.55° E; Shanxi Province), and Hohhot (40.81° N, 111.68° E; Inner Mongolia Autonomous Region). We used the Gridded Population of the World dataset for 2015 (version 4, http://sedac.ciesin.columbia.edu/data/collection/gpw-v4) to calculate the population-weighted $PM_{2.5}$ concentrations (Text S1) from our simulations to evaluate the effect of ERMs on population health.

2.5 Sensitivity simulations

We conducted six sensitivity simulations to examine the impacts of the ERMs on air quality in the NCP for December 2 to 10, 2015. Table 3 summarizes the setup of the sensitivity experiments. The ERM experiments was the control experiment, reflecting our best knowledge of the actual event. We used the simulated differences between the NOERM and the ERM experiments to evaluate the effects of the ERMs on $PM_{2.5}$ concentrations over the NCP. The simulated differences between the ERM and ERM_NOBJ experiments and the simulated differences between the NOERM and the NOERM_NOBJ experiments indicated the impacts of emissions from Beijing with and without the ERMs, respectively. The simulated differences between the ERM and ERM_NOOTH experiments and the simulated differences between the NOBJ and the NOERM_NOOTH experiments indicated

306 the impacts of emissions from other provinces/cities in the NCP with and without the ERMs,
307 respectively.

308

309 **3. Results and discussions**

310 **3.1 Simulation of the severe haze pollution event**

311 **3.1.1 Meteorological conditions during the severe haze pollution event**

312 Fig 2 shows the observed synoptic meteorological conditions during December 2 to 10, 2015.
313 Between December 2 and 4 (hereafter referred to as the clean period), the NCP was affected by a
314 mid-latitude cyclone moving across Northeastern China to Northern Japan. The passage of the cold
315 front and the intrusion of cold, clean air masses ventilated the boundary layer over the NCP with
316 northwesterly winds, resulting in the lower $PM_{2.5}$ concentrations (< 60 μg m^{-3}) during this period.
317 During Stage I (16:00 UTC of December 6 and 23:00 UTC of December 7), the NCP was under the
318 influence of a stagnant high-pressure system, which led to weak southwesterly winds, compressed
319 boundary layer, and consequently the accumulation of $PM_{2.5}$ over the NCP. During Stage II (23:00
320 UTC of December 7 and 04:00 UTC of December 10), the conditions over the NCP continued to be
321 stagnant with high relative humidity, which was not only unfavorable to pollutant dispersion but
322 also conducive to secondary $PM_{2.5}$ production. Finally, on December 10, a weak cold front passed
323 through the NCP and ventilated the boundary layer, terminating the severe haze event.

324 We verified that the model correctly simulated the progression of the meteorological conditions
325 associated with the haze event during December 2 to 10, 2015. Fig S2 shows that our model
326 correctly reproduced the observed changes in the planetary boundary layer heights (PBLHs) around
327 the NCP from >1 km during the clean period to 0.1 to 0.8 km during the polluted period. The
328 simulated surface temperatures, relative humidity, wind speeds, and wind directions also agreed
329 well with observations at the Beijing Capital International Airport (BCIA; 40.08° N, 116.59° E, Fig
330 S3) and at other surface sites in the NCP (not shown).

331

332 **3.1.2 Observed and simulated surface $PM_{2.5}$ over the NCP**

333 Fig 3 shows the observed hourly surface $PM_{2.5}$ concentrations averaged over sites in Beijing,
334 Tianjin, Hebei, Henan, and Shandong, respectively. During December 2 to 4, the observed $PM_{2.5}$

concentrations across the NCP were generally less than 80 μg m^{-3}. Observed $PM_{2.5}$ concentration began to rise on December 5 and continued to do so through Stages I and II, peaking at approximately 300 μg m^{-3} on December 9 in most cities and provinces in the NCP. The exception was the Shandong province, where the observed $PM_{2.5}$ peaked at approximately 200 μg m^{-3} on December 10.

Fig 3 also shows the simulated surface $PM_{2.5}$ concentrations at the five cities and provinces in the NCP using the reduced anthropogenic emissions associated with the ERMs. Our simulation captured the temporal variation of $PM_{2.5}$ between December 2 and 10 in Beijing, Tianjin, Hebei, Henan, and Shandong. The correlation coefficients (R) between the observed and simulated hourly $PM_{2.5}$ concentrations ranged from 0.80 to 0.95 for the five cities and provinces. The model showed good skills in reproducing the observed $PM_{2.5}$ concentrations in Beijing, Hebei, and Henan. The model overestimated the $PM_{2.5}$ concentrations during the polluted period in Tianjin and Shandong by 40% and 50%, respectively, likely due to an overestimation of local anthropogenic emissions.

Fig 4a compares the spatial distribution of the simulated surface $PM_{2.5}$ concentrations in the ERM experiment during Stages I and II against those observed. The spatial distribution of the simulated $PM_{2.5}$ concentrations was consistent with that of the observations, with high $PM_{2.5}$ concentrations exceeding 200 μg m^{-3} extending from the Henan province northward to Beijing. In Fig 4a, the simulation showed a hot spot in Tianjin that was not in the observation, likely indicating an overestimation of industrial emissions in Tianjin.

Fig 5 further compares the simulated $PM_{2.5}$ concentrations and compositions from the ERM experiment against measurements at the CRAES and PKUERS sites in Beijing during December 2 to 10, 2015. The simulated $PM_{2.5}$ concentrations in the ERM experiment agreed well with the measurements at the CRAES site (Fig 5a). The model captured the relative low $PM_{2.5}$ concentrations during December 2 to 5, the rise of $PM_{2.5}$ concentrations during December 5 to 10, as well as the sharp decline of $PM_{2.5}$ concentrations on December 10. The simulated peak $PM_{2.5}$ concentration of 308 μg m^{-3} was also in good agreement with the observation (317 μg m^{-3}). Fig 5c showed the observed average daily $PM_{2.5}$ compositions at the PKUERS site in Beijing for December 6 to 10. OA (including primary and secondary OA) was the largest chemical component in $PM_{2.5}$ measured at PKUERS, constituting 33% of the total $PM_{2.5}$ mass. This was followed by nitrate, sulfate, and ammonium, contributing 18%, 15%, and 11% of the total $PM_{2.5}$ mass, respectively. At PKUERS,

19% of the observed total $PM_{2.5}$ mass was unidentified, most likely constituted of dust. Fig 5d shows our simulated $PM_{2.5}$ compositions in the ERM experiment, which were in good agreement with the measurements. The model also indicated OA as the largest chemical component, followed by nitrate, sulfate, and ammonium. Our simulation indicated that 58% of the simulated $PM_{2.5}$ was of secondary origin, consistent with previous measurement studies which found that more than half of the $PM_{2.5}$ in Beijing during severe wintertime haze events were secondary (Huang et al., 2014).

To better understand the cause of the severe haze event, we examined the lifetime of $PM_{2.5}$ (τ) in the boundary layer of the NCP. For a species in a well-defined reservoir, the mass balance equation is (Jacob, 1999):

$$\frac{dm}{dt} = \sum \text{sources} + \sum \text{sinks} \qquad \text{Eq. (2)}$$

where m is the mass of the species in the reservior, dm/dt is the rate of mass change, and $\sum$sources and $\sum$sinks are the total sources and total sinks of the species, respectively. The residence time of the species in the reservoir is defined as $\tau \equiv m/\sum \text{sinks}$ (Jacob, 1999). In the case of $PM_{2.5}$ in the boundary layer of the NCP:

$$\tau \equiv \frac{m}{\sum \text{sinks}} = \frac{m}{L_{h-out}+L_{v-out}+L_{drydep}+L_{wetscav}+L_{chem}} \qquad \text{Eq. (3)}$$

where m was the total $PM_{2.5}$ mass in the atmospheric boundary layer of the NCP. The denominator in Eq. (3) was the sum of rates of $PM_{2.5}$ mass removal from the NCP boundary layer, which included removal by horizontal ventilation ($L_{h\text{-}out}$), vertical ventilation ($L_{v\text{-}out}$, including large-scale vertical advection and convective transport), dry deposition (L_{drydep}), wet scavenging ($L_{wetscav}$), and chemical loss (L_{chem}). We diagnosed the individual terms in Eq. (3) using the NOERM simulation for the clean and polluted periods, respectively (Table S3). There was no rainfall over the NCP during both periods, so $L_{wetscav}$ was 0. The chemical loss of $PM_{2.5}$ (L_{chem}) has been shown to be two orders of magnitude smaller than the removal rates of ventilation and deposition, especially in winter (Guth et al., 2018; Huang et al., 2019). The simulated mass of $PM_{2.5}$ in the boundary layer of the NCP averaged during the clean and polluted periods were 7.3×10^{16} μg and 1.0×10^{17} μg, respectively.

During the clean period, horizontal ventilation by the northwesterly wind was strong throughout the NCP. By applying the numbers in Table S3 into Eq. (3), we estimated a lifetime of 0.9 day for $PM_{2.5}$ in the boundary layer of the NCP. In comparison, the horizontal ventilation of $PM_{2.5}$ was much weaker under the stagnant conditions during the polluted period. As such, the

lifetime of $PM_{2.5}$ in the boundary layer of the NCP during the polluted period (Stages I and II) dramatically lengthened to 4.8 days. This led to significant accumulation of $PM_{2.5}$ in the boundary layer of the NCP.

3.2. Effects of the ERMs on surface $PM_{2.5}$ concentrations over the NCP

Fig 4b and 4c show the differences in simulated surface $PM_{2.5}$ concentrations between the NOERM and the ERM experiments during Stages I and II, which represent the effects of the ERMs on surface $PM_{2.5}$ concentrations. During Stage I (Fig 4b), most areas across the NCP saw only a 2% to 8% decline in surface $PM_{2.5}$ as a result of the ERMs. During Stage II, the decline of $PM_{2.5}$ exceeded 8% and was statistically significant (relative to the hourly variability) around Beijing, Tianjin, and the industrial areas of southern Hebei and northern Henan. The decrease of $PM_{2.5}$ was much smaller over Shandong, where the reduction in anthropogenic pollutant emissions associated with ERMs were less than 10% (Table 2). Overall, the effects of the ERMs were modest, reducing the mean $PM_{2.5}$ over the NCP by 2.5% during Stage I and by 4.2% during Stage II.

Fig 5a compares the simulated $PM_{2.5}$ concentrations in the NOERM and ERM experiments at the CREAS site in Beijing. The mean abatements in the simulated $PM_{2.5}$ concentrations at this site due to the ERMs were 3% and 10% during Stage I and Stage II, respectively. The largest simulated abatement of 11% occurred on December 9, reflecting the cumulative effect of emission reductions up to that time. Fig 5b shows the reduction of individual $PM_{2.5}$ components at the CREAS site. The reduction in secondary aerosols accounted for over 53% of the total $PM_{2.5}$ decrease during the polluted period, including most importantly SOA (-10 $\mu g\ m^{-3}$). Primary OA and EC were reduced by 8 $\mu g\ m^{-3}$ and 5 $\mu g\ m^{-3}$, respectively. Although there was a significant reduction of anthropogenic dust emissions due to the ERMs, the resulting change in $PM_{2.5}$ concentrations attributable to dust was only 7% due to its small share in the total $PM_{2.5}$ during the haze event. Fig 5c-e compare the simulated $PM_{2.5}$ composition in the ERM and NOERM experiments against the observations at the PKUERs site. Although the implementation of ERMs resulted in varying amounts of concentration decrease in different chemical species (Fig. 5b), the overall composition in the ERM and NOERM experiments remained similar, as the total $PM_{2.5}$ concentration reduction was small.

We also calculated the population-weighted $PM_{2.5}$ concentrations from our simulations to

evaluate the effect of ERMs on population health. Fig 6 compares the simulated daily $PM_{2.5}$ concentrations and $PPM_{2.5}$ concentrations from the NOERM and the ERM experiments for each of the five administrative areas for December 6 to 10. The mean reductions of $PM_{2.5}$ ($PPM_{2.5}$) attributable to the ERMs over Beijing, Tianjin, Hebei, Henan and Shandong during the polluted period (Stages I and II) were 7% (11%), 7% (7%), 5% (6%), 4% (4%), and 3% (3%), respectively. The largest decrease of daily $PM_{2.5}$ was 9% in Beijing and Tianjin. The largest decrease of daily $PPM_{2.5}$ of 14% was also in Beijing, indicating that the benefit of the ERMs in reducing public $PM_{2.5}$ exposure was greatest in the most densely-populated locations.

Overall, the reductions in $PM_{2.5}$ and $PPM_{2.5}$ as a result of the ERMs were surprisingly modest in the NCP, considering that the emissions of $PM_{2.5}$ and its precursors were significantly reduced by 8% to 48% due to the implementation of the ERMs (Table 2). In the sections below, we examined the causes for the ineffectiveness of the ERM in reducing $PM_{2.5}$ concentrations over the NCP during this severe winter haze event.

3.3. Spatial source attribution of $PM_{2.5}$ in the NCP during clean and polluted periods

We used sensitivity simulations (Table 3) to quantify the relative contributions of local versus regional emissions to $PM_{2.5}$ concentrations in Beijing and in the rest of the NCP (Tianjin, Hebei, Henan and Shandong) during the severe haze event. Using model simulations driven by Chinese anthropogenic emissions for the year 2010, Zhang et al. (2015) previously found that 50% of the monthly mean $PM_{2.5}$ concentration in Beijing in January 2013 was due to emissions within Beijing. However, this number should be re-evaluated, as there have been substantial changes in the annual anthropogenic pollutant emissions in Beijing and its surrounding areas between the 2010 inventory (Zhang et al., 2009; Lei et al., 2011; Lu et al., 2011) used by Zhang et al. (2015) and the 2016 inventory (Li et al., 2017) used in our study (Fig. S4).

Fig 7a shows the percentages of the $PM_{2.5}$ in Beijing attributable to emissions from Beijing, from the rest of the NCP and from outside the NCP, respectively. During the clean period, 60% of the simulated mean $PM_{2.5}$ concentration in Beijing was due to emissions from outside the NCP. This was mostly dust transported to Beijing by northwesterly winds. Pollutants emitted within Beijing

451 and pollutants emitted from the rest of the NCP contributed only 25% and 15% of the $PM_{2.5}$ in
452 Beijing, respectively, during the clean period. During polluted periods and basing on the NOERM
453 simulation, pollutants emitted within Beijing contributed only 18% to 22% of the $PM_{2.5}$ in Beijing
454 during Stages I and II, much lower than the 50% inferred by Zhang et al. (2015) for January 2013.
455 In comparison, pollutants emitted from the rest of the NCP and from outside the NCP contributed
456 49% to 58% and 23% to 29% of the $PM_{2.5}$ in Beijing, respectively. However, Han and Zhang (2017)
457 got similar results in July, 2015 that Beijing local emissions contributed 20% to 30% to the $PM_{2.5}$
458 concentrations in Beijing and the surrounding regions contributed the majority. The large
459 contribution of pollutants emitted from outside Beijing to the $PM_{2.5}$ in Beijing during the severe
460 haze event reflected the regional stagnant weather, which enabled the accumulation of pollutants
461 over the entire NCP.

462 Due to the implementation of ERMs, the simulated mean $PM_{2.5}$ concentrations in Beijing
463 decreased by 4% and 9% relative to the NOERM case during Stages I and II, respectively. During
464 Stage I, the decrease was due to the combined effects of ERMs implemented in Beijing (2%) and in
465 the rest of the NCP (2%). During Stage II, the decrease was mostly due to the combined effects of
466 ERMs implemented in Beijing (5%) and the rest of the NCP (3%). A remaining 1% decrease of the
467 $PM_{2.5}$ concentration in Beijing during State II was due to small nonlinearity in the $PM_{2.5}$ production.
468 We will return to this point later.

469 Fig 7b shows the simulated attribution of the mean $PM_{2.5}$ concentration in the rest of the NCP.
470 Under both clean and polluted conditions, more than 62% of the mean $PM_{2.5}$ concentrations in the
471 rest of the NCP was from local emissions, while 34% to 37% was attributed to emissions from
472 outside the NCP. Contributions from Beijing were small throughout the study period. The simulated
473 mean concentrations of $PM_{2.5}$ in the rest of the NCP decreased by 3% and 5% in the ERM case
474 relative to the NOERM case during Stages I and II, respectively. All of the simulated abatements in
475 $PM_{2.5}$ were attributed to emission reductions in the rest of the NCP.

476 Our sensitivity simulations used the "emission zero-out" approach to quantify the percent
477 contribution of a particular source area to the $PM_{2.5}$ concentration in a receptor area. For example,
478 we compared the simulated Beijing $PM_{2.5}$ concentrations between the ERM and ERM_NOOTH
479 experiments to quantify the contribution of emissions from the rest of the NCP to the $PM_{2.5}$

concentrations in Beijing. One concern for this approach is that secondary $PM_{2.5}$ production is nonlinear, and that zeroing-out the emissions from a source area may cause nonlinear chemical responses to the simulated $PM_{2.5}$ concentrations in the receptor area. Another potential source of nonlinearity involves the feedback between $PM_{2.5}$ and meteorology, but that was not an issue in our case because our WRF-Chem simulations were nudged with meteorological observations. We found however, that the overall nonlinear chemical responses was small in this particular pollution event. Using the "emission zero-out" approach, we estimated that the pollutants from Beijing and from the rest of the NCP contributed 29.7 and 89.4 μg m^{-3} of $PM_{2.5}$ in Beijing under the NOERM scenario during Stage I (Fig. 7a). This meant that the $PM_{2.5}$ contributed from outside the NCP was 36.1 μg m^{-3} under the NOERM scenario during Stage I. Under the ERM scenario, we similarly calculated a 36.3 μg m^{-3} contribution from outside the NCP. This indicated that, during this particular pollution event, there was no strong nonlinearity in $PM_{2.5}$ production, otherwise the perturbation in emissions by the ERM enforcement would have led to differences in the calculated contribution from outside the NCP, where no control measures was implemented. We further compared the sensitivity simulations for Beijing and for the NCP during Stages I and II. Overall, the chemical nonlinearity accounted for, at most a 1% decrease in the $PM_{2.5}$ concentration in Beijing during Stage II under the ERM scenario. This small nonlinearity did not change our overall source attribution.

3.4. Cause of the ineffectiveness of the ERMs during the severe haze event of December 6 to 10, 2015

We analytically examined the cause of the ineffectiveness of the ERMs in abating surface $PM_{2.5}$ concentrations over the NCP during December 6 to 10, 2015. Without the ERMs implemented, the daily source of $PM_{2.5}$ contributed by source area j to a specific receptor area i during the polluted period was $S_{NOERM,i,j}$ (μg m^{-3} day^{-1}), which included contributions of both primary and secondary from source area j. The total daily $PM_{2.5}$ source for a receptor area i ($S_{NOERM,i}$) was the sum of $S_{NOERM,\,i,\,j}$ over all values of j. In our case, j = 1 to 3, indicating contributions from Beijing (j = 1), from the rest of the NCP (j = 2), and from all other regions outside the NCP (j = 3), respectively:

$$S_{\mathrm{NOERM},i} = \sum_{j=1}^{3} S_{\mathrm{NOERM},i,j} \qquad \text{Eq. (3a)}$$

The individual $S_{\mathrm{NOERM},\,i,\,j}$ can also be expressed as:

$$S_{\mathrm{NOERM},i,j} = g_{i,j} \cdot S_{\mathrm{NOERM},i} \qquad \text{Eq. (3b)}$$

where $g_{i,j}$ was the fractional contribution of pollutants from source area j to surface $PM_{2.5}$ in receptor area i. The values $g_{i,j}$ for j = 1, 3 were given by the source attribution in Section 5 (Fig. 7). For the receptor area Beijing, the values of $g_{i,j}$ for j = 1, 3 were 0.19, 0.58, and 0.23 during Stage I and 0.22, 0.49, 0.29 during Stage II. Similarly, for the receptor area of the rest of the NCP, the values of $g_{i,j}$ for j = 1, 3 were 0.01, 0.65, and 0.34 during Stage I and 0.01, 0.62, and 0.37 during Stage II.

For a well-defined receptor area i, $S_{\mathrm{NOERM},i}$ was also equal to the sum of the inflow of $PM_{2.5}$ from other source areas, the local primary $PM_{2.5}$ emissions, and the local chemical production of secondary $PM_{2.5}$:

$$S_{\mathrm{NOERM},i} = s_{\mathrm{NOERM},i}|_{\mathrm{PM_{2.5}\ inflow}} + s_{\mathrm{NOERM},i}|_{\mathrm{local\ primary\ PM_{2.5}\ emis}} + s_{\mathrm{NOERM},i}|_{\mathrm{local\ secondary\ PM_{2.5}\ prod}} \qquad \text{Eq. (4)}$$

The first two terms on the right-hand-side in Eq. (4) can be directly calculated from our NOERM simulation. The third term involves the efficiencies at which precursors were converted to secondary $PM_{2.5}$. We estimate this third term using the simulated local conversion ratios of individual anthropogenic precursors to their respective secondary aerosol products. For example, we used the simulated local sulfur oxidation ratio (SOR) ≡ $[SO_4^{2-}\,(a)]$ / ($[SO_4^{2-}\,(a)]$ + $[SO_2\,(g)]$) to estimate the local conversion efficiency of SO_2 to sulfate (Fang et al., 2017). Similarly, the local nitrogen oxidation ratio (NOR), the local ammonia conversion ratio (NHR), and the anthropogenic VOC oxidation ratio (VOR) were calculated from our NOERM simulation (Fang et al., 2017). The definitions and values of these ratios are shown in Table S4. Our simulated SOR, NOR, and NHR values were in the range of values previously reported in wintertime observation studies over the NCP (Liu et al., 2020). Using the model emissions and the values in Table S4, we estimated the third term on the right-hand-side of Eq. (4) as:

$$s_{\mathrm{NOERM},i}|_{\mathrm{local\ secondary\ PM_{2.5}\ prod}} = E_{SO_2,i} \cdot \mathrm{SOR}_i + E_{NO_x,i} \cdot \mathrm{NOR}_i + E_{NH_3,i} \cdot \mathrm{NHR}_i + E_{\mathrm{VOC},i} \cdot \mathrm{VOR}_i \qquad \text{Eq. (5)}$$

Using the NOERM simulated results to calculate the values in Eqs. (4) and (5), we estimated

535 $S_{NOERM,i}$ to be 68 μg m^{-3} day^{-1} in Beijing and 76 μg m^{-3} day^{-1} for the rest of the NCP during the
536 polluted period.

537 We assumed that the transport pathways and transport efficiencies of $PM_{2.5}$ and the production
538 efficiencies of secondary $PM_{2.5}$ from precursors during the polluted period were similar with and
539 without the implementation of ERMs for a given period. I.e., we assumed that the values of $g_{i,j}$ and
540 the conversion ratios in Table S4 were similar with and without the implementation of ERMs for a
541 given period. This is a reasonable assumption given that the simulated impacts of the ERMs on
542 $PM_{2.5}$ concentrations were small across the NCP. Also, our sensitivity simulations indeed showed
543 the source attributions ($g_{i,j}$) to be very similar with and without the ERMs (Fig. 7). Then, the
544 fractional abatement of the total $PM_{2.5}$ source contributed from source area j to any other receptor
545 area, α_j, was:

546 $$\alpha_j = \frac{S_{\mathrm{NOERM},i,j} - S_{\mathrm{ERM},i,j}}{S_{\mathrm{NOERM},i,j}} = \frac{E_{\mathrm{NOERM},j} - E_{\mathrm{ERM},j}}{E_{\mathrm{NOERM},j}} \quad \text{Eq. (6)}$$

547 where $S_{ERM,i,j}$ was the daily source of $PM_{2.5}$ contributed by source area j to a specific receptor area
548 i during the polluted period with the ERM implemented. $E_{NOERM,j}$ and $E_{ERM,j}$ were the emission rates
549 of precursors from source area j. Table 2 shows the emission reduction percentages of primary $PM_{2.5}$
550 and precursors to be in the range of 4% and 15% during Stage I. We estimated the overall α_j by
551 weighting the precursor emission reduction percentages with the simulated composition of $PM_{2.5}$
552 (Fig. 5e). In this way, we estimated α_j to be 12% and 34% for Beijing during Stages I and II,
553 respectively. Using the same method, the values of α_j were estimated to be 11% and 14% for the
554 rest of NCP during Stages I and II, respectively.

555 Finally, if the ERMs were implemented, the total daily source of $PM_{2.5}$ in area i during the
556 polluted period was $S_{ERM,i}$:

557 $$S_{\mathrm{ERM},i} = \sum_{j=1}^{3} \left[\left(1 - \alpha_j\right) \cdot g_{i,j} \right] \cdot S_{\mathrm{NOERM},i} \quad \text{Eq. (7)}$$

558 For region i and from an initial $PM_{2.5}$ concentration $c_i(t = t_0)$ in the boundary layer, if ERMs were
559 not implemented, the $PM_{2.5}$ concentration ($c_{NOERM,i}$) at time $t = t_0 + \Delta t$ during the polluted period
560 was (Jacob, 1999):

561 $$c_{\mathrm{NOERM},i}(t_0 + \Delta t) = c_i(t_0) \cdot e^{-\Delta t/\tau_i} + S_{\mathrm{NOERM},i} \cdot \tau_i \left(1 - e^{-\Delta t/\tau_i}\right) \quad \text{Eq. (8)}$$

where τ_i is the lifetime of $PM_{2.5}$ in region i, which was 4.8 days throughout the NCP during the polluted period. If ERMs were implemented, the $PM_{2.5}$ concentration ($c_{ERM,i}$) at time $t = t_0 + \Delta t$ during the polluted period was:

$$c_{\mathrm{ERM},i}(t_0 + \Delta t) = c_i(t_0) \cdot e^{-\Delta t/\tau_i} + S_{\mathrm{ERM},i} \cdot \tau_i\left(1 - e^{-\Delta t/\tau_i}\right) \quad \text{Eq. (9)}$$

Eqs. (8) and (9) thus give the analytical solution of how the $PM_{2.5}$ concentrations change with time given the initial concentration ($c_i(t_0)$), the $PM_{2.5}$ source ($S_{\mathrm{NOERM},i}$ or $S_{\mathrm{ERM},i}$), and the lifetime of $PM_{2.5}$ (τ_i) in the reservoir (boundary layer of NCP). At time $t = t_0 + \Delta t$, the analytical solution of the fractional abatement of $PM_{2.5}$ in area i associated with the implementation of the NCP-wide ERMs was:

$$f_i = \frac{c_{\mathrm{NOERM},i}(t_0+\Delta t) - c_{\mathrm{ERM},i}(t_0+\Delta t)}{c_{\mathrm{NOERM},i}(t_0+\Delta t)} \quad \text{Eq. (10)}$$

where $c_{NOERM,i}(t_0 + \Delta t)$ and $c_{ERM,i}(t_0 + \Delta t)$ were described analytically by Eqs (8) and (9), respectively.

Using Eqs (8), (9), and (10), we can analytically compute the fractional abatements of $PM_{2.5}$ concentrations (f_i) in Beijing and in the rest of NCP as a result of the enforced ERMs, as functions of days since the initiation of the ERM enforcement (Δt). The results are shown in Fig. 8. The fractional abatements of $PM_{2.5}$ gradually become more evident over time. The rates of changes of f_i were determined not only by the emission reductions, but also by the lifetimes of $PM_{2.5}$, as indicated in Eqs. (8) to (10). In Beijing, the mean analytical fractional abatements of $PM_{2.5}$ during Stages I and II were 4% and 9%, respectively (Fig 8a). In the rest of the NCP, the mean analytical fractional abatement of $PM_{2.5}$ during Stages I and II were 3% and 6%, respectively (Fig 8b). These analytically calculated mean fractional abatements of $PM_{2.5}$ were consistent with our simulated results in Section 3.3.

As calculated in Section 3.1.2, the lifetime of $PM_{2.5}$ in the boundary layer of the entire NCP (τ_i) was 4.8 days during the polluted periods. Hypothetically, if the lifetime of $PM_{2.5}$ were very short, or if the ERMs were enforced for a duration (Δt) much longer than τ_i, then $\Delta t/\tau_i \rightarrow \infty$ and $exp(-\Delta t/\tau_i)$ would approach 0 in Eqs. (8) and (9). Under this hypothetical situation, the fractional abatement (f_i) of $PM_{2.5}$ in area i associated with the implementation of the NCP-wide ERMs would approach a maximum, $f_{max,i}$:

$$f_{max,i} = \frac{m_{\mathrm{NOERM},i}(\infty) - m_{\mathrm{ERM},i}(\infty)}{m_{\mathrm{NOERM},i}(\infty)}$$

$$= \frac{c_i(t_0)\cdot e^{-\infty} + S_{\mathrm{NOERM},i}\cdot\tau_i(1-e^{-\infty}) - \left[c_i(t_0)\cdot e^{-\infty} + S_{\mathrm{ERM},i}\cdot\tau_i(1-e^{-\infty})\right]}{c_i(t_0)\cdot e^{-\infty} + S_{\mathrm{NOERM},i}\cdot\tau_i(1-e^{-\infty})}$$

$$\rightarrow \frac{S_{\mathrm{NOERM},i}-S_{\mathrm{ERM},i}}{S_{\mathrm{NOERM},i}} = 1 - \sum_{j=1}^{3}\left[\left(1-\alpha_j\right)\cdot g_{i,j}\right] \qquad \text{Eq. (11)}$$

By applying the values α_j (estimated by weighting the emission reductions in Table 2, as described above) and $g_{i,j}$ (from Fig. 7), one can calculate the values of $f_{max,i}$. For Beijing, $f_{max,i}$ were 9% and 15% during Stages I and II, respectively. For the rest of NCP, $f_{max,i}$ were 8% and 9% during Stages I and II, respectively.

These results explained the ineffectiveness of the ERMs in alleviating surface $PM_{2.5}$ pollution during December 6 to 10, 2015. If, hypothetically, the stagnant weather and the same ERM enforcement for Stage II had continued, then the fractional abatements of $PM_{2.5}$ would have eventually approached $f_{max,i}$ after approximately 10 days (2τ). This is shown in Fig. 8 by the f_i curves eventually approaching the $f_{max,i}$ values, which were 15% and 9% for Beijing and the rest of the NCP, respectively. In reality, however, the passage of a cold front ventilated the NCP boundary layer on December 10, 2015 and terminated the severe haze event. Thus, there was insufficient time for the $PM_{2.5}$ concentrations to fully reflect the reduction in emissions, i.e., the fractional abatements of $PM_{2.5}$ have not had enough time to reach their maximum potential values, $f_{max,i}$.

4. Conclusions

During December 6 to 10, 2015, for the first time, the cities and provinces in the NCP executed ERMs to reduce anthropogenic emissions, with the goal of alleviating a severe $PM_{2.5}$ pollution event. We simulated the $PM_{2.5}$ concentrations in the NCP before and during this event, both with and without the anthropogenic emission reductions associated with the ERMs, to evaluate the effectiveness of the ERMs. We surveyed provincial/municipal documents and news reports to determine the reductions of pollutant emissions due to the ERMs in each of the five cities and provinces in the NCP. With the exception of NH_3, the emissions of anthropogenic $PM_{2.5}$ and its precursors were reduced by 8% to 48% across the NCP as a result of the ERMs. Our model

615 simulation using the reduced emissions was able to reproduce the observed $PM_{2.5}$ concentrations
616 and compositions throughout the event.

617 We found that the effects of the ERMs on $PM_{2.5}$ concentrations in the NCP were surprisingly
618 modest. Overall, the mean abatement of $PM_{2.5}$ during the polluted period attributable to the ERMs
619 were 7% in Beiijng and 4% for the rest of the NCP. We found that, during the polluted period, only
620 18% to 22% of the surface $PM_{2.5}$ in Beijing was attributable to local emissions. Pollutants emitted
621 from the rest of the NCP and from outside the NCP contributed 49% to 58% and 23% to 29% of the
622 $PM_{2.5}$ in Beijing, respectively, during the polluted period. For the rest of the NCP, more than 62%
623 of the mean surface $PM_{2.5}$ was from local emissions, while 34% to 37% was attributed to emissions
624 from outside the NCP.

625 We found that the ineffectiveness of the ERMs in alleviating the high $PM_{2.5}$ concentrations was
626 due to the lengthened lifetime of $PM_{2.5}$ (5 days) in the boundary layer of the NCP, which was in turn
627 due to slowed horizontal and vertical ventilation under the stagnant weather conditions. As a result,
628 there was insufficient time for the $PM_{2.5}$ concentrations to fully reflect the reduction in emissions
629 and the efficacy of the ERMs were finished. This is in vast contrast against previous occasions when
630 temporary emission controls implemented in the BTH and surrounding areas had significantly
631 improved the air quality in Beijing, such as during the Sino-African Summit, the Beijing Olympic
632 Games, the APEC Summit, and the 2015 Chinese Miliary Parade (e.g.,Cheng et al., 2008; S. Wang
633 et al., 2010; Liu et al., 2015; Zhang et al., 2016; G. Wang et al., 2017). On those occasions, emission
634 controls were enforced for a longer period of time. More importantly, the efficacy of temporary
635 emission control actions were aided by the effective ventilation of the boundary layer air in Beijing
636 (e.g., Zhang et al., 2016).

637 Our result showed the challenge in reducing surface $PM_{2.5}$ concentrations during severe
638 wintertime haze events by implementing ERMs, because the stagnant weather conditions would
639 impede the efficacy of the ERMs. As a result, anthropogenic emissions in the NCP during severe
640 wintertime haze events would need to be reduced by a much larger percentage if more pronounced
641 abatements of surface $PM_{2.5}$ concentrations were desired. Such large emission reductions would be
642 economically costly. Concurrently, stronger advisory to citizens to reduce outdoor activities and to
643 improve indoor air quality (e.g., using air purifiers to remove $PM_{2.5}$) is also necessary to effectively

reduce public exposure to high $PM_{2.5}$ in the NCP during these severe wintertime haze events.

Acknowledgment

This work was supported by the Ministry of Science and Technology of China (2017YFC0209802) and by the National Natural Sciences Foundation of China (41975158). J. Guo was supported by the National Natural Sciences Foundation of China under Grant 41771399. Y. Zhang was supported by the National Natural Sciences Foundation of China under Grant 41675121.

References

Carter, W.P.L., 2000. Implementation of the SAPRC99 chemical mechanism into the Models-3 framework. Report to the U.S. EPA. Statewide Air Pollution Research Center, University of California, Riverside, CA, USA.

Chen, R., Zhao, Z., and Kan, H., 2013. Heavy smog and hospital visits in Beijing, China. Am. J. Respir Crit. Care. Med. 188, 1170-1171. DOI: 10.1164/rccm.201304-0678LE.

Chen, Z., Chen, D., Wen, W., Zhuang, Y., Kwan, M.-P., Chen, B., Zhao, B., Yang, L., Gao, B., Li, R., and Xu, B., 2019. Evaluating the "2 + 26" regional strategy for air quality improvement during two air pollution alerts in Beijing: variations in $PM_{2.5}$ concentrations, source apportionment, and the relative contribution of local emission and regional transport. Atmos. Chem. Phys. 19, 6879-6891. DOI: 10.5194/acp-19-6879-2019.

Cheng, Y.F., Heintzenberg, J., Wehner, B., Wu, Z.J., Su, H., Hu, M., and Mao, J.T., 2008. Traffic restrictions in Beijing during the Sino-African Summit 2006: aerosol size distribution and visibility compared to long-term in situ observations. Atmos. Chem. Phys. 8, 7583-7594. DOI: 10.5194/acp-8-7583-2008.

Cheng, Y.F., Zheng, G., Wei, C., Mu, Q., Zheng, B., Wang, Z., Gao, M., Zhang, Q., He, K., Carmichael, G., Pöschl, U., and Su, H., 2016. Reactive nitrogen chemistry in aerosol water as a source of sulfate during haze events in China. Sci. Adv. 2 (12), e1601530. DOI: 10.1126/sciadv.1601530.

671 Dang, R., and Liao, H., 2019. Severe winter haze days in the Beijing–Tianjin–Hebei region from
672 1985 to 2017 and the roles of anthropogenic emissions and meteorology. Atmos. Chem. Phys.
673 19, 10801-10816. DOI: 10.5194/acp-19-10801-2019.

674 Emmons, L.K., Walters, S., Hess, P.G., Lamarque, J.-F., Pfister, G.G., Fillmore, D., Granier, C.,
675 Guenther, A., Kinnison, D., Laepple, T., Orlando, J., Tie, X., Tyndall, G., Wiedinmyer, C.,
676 Baughcum, S.L., and Kloster, S., 2010. Description and evaluation of the Model for Ozone
677 and Related chemical Tracers, version 4 (MOZART-4). Geosci. Model Dev. 3, 43-67. DOI:
678 10.5194/gmd-3-43-2010.

679 Fang, C., Zhang, Z., Jin, M., Zou, P., and Wang, J., 2017. Pollution characteristics of $PM_{2.5}$ aerosol
680 during haze periods in Changchun, China. Aerosol Air Qual. Res. 17, 888-895. DOI:
681 10.4209/aaqr.2016.09.0407.

682 Fu, T.-M., Jacob, D.J., and Heald, C.L., 2009. Aqueous-phase reactive uptake of dicarbonyls as a
683 source of organic aerosol over eastern North America. Atmos. Environ. 43 (10), 1814-1822.
684 DOI: 10.1016/j.atmosenv.2008.12.029.

685 Fu, T.-M., Jacob, D.J., Wittrock, F., Burrows, J.P., Vrekoussis, M., and Henze, D.K., 2008. Global
686 budgets of atmospheric glyoxal and methylglyoxal, and implications for formation of
687 secondary organic aerosols. J. Geophys. Res. 113, D15303. DOI: 10.1026/2007JD009505.

688 Gao, J., Peng, X., Chen, G., Xu, J., Shi, G., Zhang, Y., and Feng, Y., 2016. Insights into the
689 chemical characterization and sources of $PM_{2.5}$ in Beijing at a 1-h time resolution. Sci. Total.
690 Environ. 542, 162-171. DOI: 10.1016/j.scitotenv.2015.10.082.

691 Georgiou, G.K., Christoudias, T., Proestos, Y., Kushta, J., Hadjinicolaou, P., Lelieveld, J., 2018.
692 Air quality modelling in the summer over the Eastern Mediterranean using WRF/Chem:
693 chemistry and aerosol mechanisms intercomparison. Atmos. Chem. Phys. 18, 1555–1571.
694 DOI: 10.5194/acp-18-1555-2018.

695 Gilliam, R.C., Godowitch, J.M., and Rao, S.T., 2012. Improving the horizontal transport in the
696 lower troposphere with four dimensional data assimilation. Atmos. Environ. 53, 186-201.
697 DOI: 10.1016/j.atmosenv.2011.10.064.

Ginoux, P., Chin, M., Tegen, I., Prospero, J.M., Holben, B., Dubovik, O., and Lin, S.-J., 2001. Sources and distribution of dust aerosols simulated with the GOCART model. J. Geophys. Res. Atmos. 106, 20255–20273. DOI: 10.1029/2000JD000053.

Grell, G.A., Peckham, S.E., Schmitz, R., Mckeen, S.A., Frost, G., Skamarock, W.C., and Eder, B., 2005. Fully coupled "online" chemistry within the WRF model. Atmos. Environ. 39 (37), 6957-6975. DOI: 10.1016/j.atmosenv.2005.04.027.

Guenther, A., Karl, T., Harley, P., Wiedinmyer, C., Palmer, P.I., and Geron, C., 2006. Estimates of global terrestrial isoprene emissions using MEGAN (model of emissions of gases and aerosols from nature). Atmos. Chem. Phys. 6, 3181-3210. DOI: 10.5194/acp-6-3181-2006.

Guo, J., He, J., Liu, H., Miao, Y., Liu, H., and Zhai, P., 2016a. Impact of various emission control schemes on air quality using WRF-Chem during APEC China 2014. Atmos. Environ. 140, 311–319. DOI: 10.1016/j.atmosenv.2016.05.046.s.

Guo, J., Miao, Y., Zhang, Y., Liu, H., Li, Z., Zhang, W., He, J., Lou, M., Yan, Y., Bian, L., and Zhai, P., 2016b. The climatology of planetary boundary layer height in China derived from radiosonde and reanalysis data. Atmos. Chem. Phys. 16, 13309–13319. DOI: 10.5194/acp-16-13309-2016.

Guth, J., Marécal, V., Josse, B., Arteta, J., and Hamer, P., 2018. Primary aerosol and secondary inorganic aerosol budget over the Mediterranean Basin during 2012 and 2013. Atmos. Chem. Phys. 18, 4911-4934. DOI: 10.5194/acp-18-4911-2018.

Han, X., and Zhang, M., 2019. Assessment of the regional source contributions to $PM_{2.5}$ mass concentration in Beijing. Atmos. Oceanic Sci. Lett. 11, 143-149. DOI: 10.1080/16742834.2018.1412796.

He, H., Wang, Y., Ma, Q., Ma, J., Chu, B., Ji, D., Tang, G., Liu, C., Zhang, H., and Hao, J., 2014. Mineral dust and NO_x promote the conversion of SO_2 to sulfate in heavy pollution days. Sci. Rep. 4, 4172. DOI: 10.1038/srep04172.

723 Huang, K., Zhang, X., and Lin, Y., 2015. The “APEC Blue” phenomenon: regional emission
724 control effects observed from space. Atmos. Res. 164-165, 65-75. DOI:
725 10.1016/j.atmosres.2015.04.018.

726 Huang, R., Zhang, Y., Bozzetti, C., Ho, K., Cao, J., Han, Y., Daellenbach, K., Slowik, J., Platt, S.,
727 Canonaco, F., Zotter, P., Wolf, R., Pieber, S., Bruns, E., Crippa, M., Ciarelli, G., Piazzalunga,
728 A., Schwikowski, M., Abbaszade, G., Schnelle-Kreis, J., Zimmermann, R., An, Z., Szidat, S.,
729 Baltensperger, U., Haddad, I., and Prévót, A., 2014. High secondary aerosol contribution to
730 particulate pollution during haze events in China. Nature 514, 218-222. DOI:
731 10.1038/nature13774.

732 Huang, W., Fang, D., Shang, J., Li, Z., Zhang, Y., Huo, P., Liu, Z., Schauer, J.J., and Zhang, Y.,
733 2018. Relative impact of short-term emissions controls on gas and particle-phase oxidative
734 potential during the 2015 China Victory Day Parade in Beijing, China. Atmos. Environ. 183,
735 49-56. DOI: 10.1016/j.atmosenv.2018.03.046.

736 Huang, W., Harald, S., Shen, X., Ramisetty, R., Leisner, T., and Mohr, C., 2019. Seasonal
737 characteristics of organic aerosol chemical composition and volatuluty in Stuttgart, Germany.
738 Atmos. Chem. Phys. 19, 11687–11700. DOI: 10.5194/acp-19-11687-2019.

739 Hung, H.M., Hsu, M.N., and Hoffmann, M.R., 2018. Quantification of SO_2 oxidation on
740 interfacial surfaces of acidic micro-droplets: implication for ambient sulfate formation.
741 Environ. Sci. Technol. 52, 9079−9086. DOI: 10.1021/acs.est.8b01391.

742 Jacob, D.J., 1999. Introduction to Atmospheric Chemistry, Princeton University Press, Princeton,
743 New Jersey, 266pp.

744 Jeong, J., and Park, R.J., 2013. Effects of the meteorological variability on regional air quality in
745 East Asia. Atmos. Environ. 69, 46-55. DOI: 10.1016/j.atmosenv.2012.11.061.

746 Kalnay, E., Kanamitsu, M., Kister, R., Collins, W., Deaven, D., Gandin, L., Iredell, M., Saha, S.,
747 White, G., Woollen, J., Zhu, Y., Chelliah, M., Ebisuzaki, W., Higgins, W., Janowiak, J., Mo,
748 K.C., Ropelewski, C., Wang, J., Leetmaa, A., Re Renold, R., Henne, R., Joseph, D., 1996.

749 The NCEP/NCAR 40-year reanalysis project. B. Am. Meteorol. Soc. 77, 437-471. DOI:
750 10.1175/1520‐0477(1996)077<0437:TNYRP>2.0.CO;2.

751 Lane, T.E., Donahue, N.M., and Pandis, S.N., 2008. Simulating secondary organic aerosol
752 formation using the volatility basis-set approach in a chemical transport model. Atmos.
753 Environ. 42, 7439-7451. DOI: 10.1016/j.atmosenv.2008.06.026.

754 LeGrand, S.L., Polashenski, C., Letcher, T.W., Creighton, G.A., Peckham, S.E., and Cetola, J.D.,
755 2019. The AFWA dust emission scheme for the GOCART aerosol model in WRF-Chem
756 v3.8.1. Geosci. Model Dev. 12, 131-166. DOI: 10.5194/gmd-12-131-2019.

757 Lei, Y., Zhang, Q., He, K.B. and Streets, D.G., 2011. Primary anthropogenic aerosol emission trends
758 for China, 1990–2005. Atmos. Chem. Phys. 11, 931-954. DOI:10.5194/acp-11-931-2011.

759 Leung, D.M., Tai, A.P.K., Mickley, L.J., Moch, J.M., van Donkelaar, A., Shen, L., and Martin,
760 R.V., 2018. Synoptic meteorological modes of variability for fine particulate matter ($PM_{2.5}$)
761 air quality in major metropolitan regions of China, Atmos. Chem. Phys. 18, 6733-6748. DOI:
762 10.5194/acp-18-6733-2018.

763 Li, J., Xie, S.D., Zeng, L.M., Li, L.Y., Li, Y.Q., and Wu, R.R., 2015. Characterization of ambient
764 volatile organic compounds and their sources in Beijing, before, during, and after Asia-
765 Pacific Economic Cooperation China 2014. Atmos. Chem. Phys. 15, 7945-7959. DOI:
766 10.5194/acp-15-7945-2015.

767 Li, M., Zhang, Q., Kurokawa, J.-I., Woo, J.-H., He, K., Lu, Z., Ohara, T., Song, Y., Streets, D.G.,
768 Carmichael, G.R., Cheng, Y., Hong, C., Huo, H., Jiang, X., Kang, S., Liu, F., Su, H., and
769 Zheng, B., 2017. MIX: a mosaic Asian anthropogenic emission inventory under the
770 international collaboration framework of the MICS-Asia and HTAP. Atmos. Chem. Phys. 17,
771 935-963. DOI: 10.5194/acp-17-935-2017.

772 Li, N., Fu, T.-M., Cao, J.J., Lee, S.C., Huang, X.F., He, L.-Y., Ho, K.-F., Fu, J.S., and Lam, Y.-F.,
773 2013. Sources of secondary organic aerosols in the Pearl River Delta region in fall:
774 contributions from the aqueous reactive uptake of dicarbonyls. Atmos. Environ. 76, 200-207.
775 DOI: 10.1016/j.atmosenv.2012.12.005.

Liu, H., He, J., Guo, J., Miao, Y., Yin, J., Wang, Y., Xu, H., Liu, H., Yan, Y., Li, Y., and Zhai, P., 2017. The blue skies in Beijing during APEC 2014: A quantitative assessment of emission control efficiency and meteorological influence. Atmos. Environ. 167, 235-244, DOI: 10.1016/j.atmosenv.2017.08.032.

Liu, J., Xie, P., Wang, Y., Wang, Z., He, H., Liu, W., 2015. Haze observation and control measure evaluation in Jing-Jin-Ji (Beijing, Tianjin, Hebei) area during the period of the Asia-Pacific Economic Cooperation (APEC) meeting. Bulletin of the Chinese Academy of Sciences 30 (3), 368−377. DOI: 10.16418/j.issn.1000-3045.2015.03.011.

Liu, M., Song, Y., Zhou, T., Xu, Z., Yan, C., Zheng, M., Wu, Z., Hu, M., Wu, Y., and Zhu, T., 2017. Fine particle pH during severe haze episodes in northern China. Geophys. Res. Lett. 44, 5213–5221, DOI: 10.1002/2017GL073210.

Liu, P., Ye, C., Xue, C., Zhang, C., Mu, Y., and Sun, X., 2020. Formation mechanisms of atmospheric nitrate and sulfate during the winter haze pollution periods in Beijing: gas-phase, heterogeneous and aqueous-phase chemistry. Atmos. Chem. Phys. 20, 4153–4165, 2020. DOI: 10.5194/acp-20-4153-2020.

Liu, T., Gong, S., He, J., Yu, M., Wang, Q., Li, H., Liu, W., Zhang, J., Li, L., Wang, X., Li, S., Lu, Y., Du, H., Wang, Y., Zhou, C., Liu, H., and Zhao, Q., 2017. Attributions of meteorological and emission factors to the 2015 winter severe haze pollution episodes in China's Jing-Jin-Ji area. Atmos. Chem. Phys. 17, 2971-2980. DOI: 10.5194/acp-17-2971-2017, 2017.

Lu, Z., Zhang, Q., and Streets, D.G., 2011. Sulfur dioxide and primary carbonaceous aerosol emissions in China and India, 1996–2010. Atmos. Chem. Phys. 11, 9839-9864. DOI: 10.5194/acp-11-9839-2011.

Ministry of Environmental Protection of the People's Republic of China, 2012. Ambient Air Quality Standards (GB3095-2012).

Ministry of Environmental Protection of the People's Republic of China, 2013. Monitoring and Warning Scheme for Heavy Pollution Weather in Beijing, Tianjin, Hebei, and Its Surrounding Areas (HF [2013] No. 111).

803 Ministry of Environmental Protection of the People's Republic of China, 2014. Report on the
804 State of the Environment in China 2013.

805 Ministry of Environmental Protection of the People's Republic of China, 2015. Report on the
806 State of the Environment in China 2014.

807 Ministry of Environmental Protection of the People's Republic of China, 2016. Report on the
808 State of the Environment in China 2015.

809 Ministry of Environmental Protection of the People's Republic of China, 2017. Report on the
810 State of the Environment in China 2016.

811 Ministry of Ecology and Environment of the People's Republic of China, 2018. Report on the
812 State of the Ecology and Environment in China 2017.

813 Ministry of Ecology and Environment of the People's Republic of China, 2019. Report on the
814 State of the Ecology and Environment in China 2018.

815 Schleicher, N., Norra, S., Chen, Y., Chai, F., and Wang, S., 2012. Efficiency of mitigation
816 measures to reduce particulate air pollution – a case study during the Olympic Summer
817 Games 2008 in Beijing, China. Sci. Total Environ. 427–428, 146-158. DOI:
818 10.1016/j.scitotenv.2012.04.004.

819 Seinfeld, J.H., and Pandis, S.N., 2006. Atmospheric Chemistry and Physics: From Air Pollution to
820 Climate Change (II), John Wiley & Sons, Inc., Hoboken, New Jersey, 963pp.

821 Shao, J., Chen, Q., Wang, Y., Lu, X., He, P., Sun, Y., Shah, V., Martin, R.V., Philip, S., Song, S.,
822 Zhao, Y., Xie, Z., Zhang, L., and Alexander, B., 2019. Heterogeneous sulfate aerosol
823 formation mechanisms during wintertime Chinese haze events: air quality model assessment
824 using observations of sulfate oxygen isotopes in Beijing. Atmos. Chem. Phys. 19, 6107-6123.
825 DOI: 10.5194/acp-19-6107-2019.

826 State Council of the People's Republic of China, 2013. Air Pollution Prevention and Control
827 Action Plan (GF [2013] No. 37).

828 Tang, R., Wu, Z., Li, X., Wang, Y., Shang, D., Xiao, Y., Li, M., Zeng, L., Wu, Z., Hallquist, M.,
829 Hu, M., and Guo, S., 2018. Primary and secondary organic aerosols in summer 2016 in
830 Beijing. Atmos. Chem. Phys. 18, 4055-4068. DOI: 10.5194/acp-18-4055-2018.

831 Tie, X., Huang, R., Cao, J., Zhang, Q., Cheng, Y., Su, H., Chang, D., Pöschl, U., Hoffmann, T.,
832 Dusek, U., Li, G., Worsnop, D., and O'Dowd, C., 2017. Severe pollution in China amplified
833 by atmospheric moisture. Sci. Rep. 7, 15760. DOI: 10.1038/s41598-017-15909-1.

834 Wang, F., Chen, D.S., Cheng, S.Y., Li, J.B., Li, M.J., and Ren, Z.H., 2010. Identification of regional
835 atmospheric PM_{10} transport pathways using HYSPLIT, MM5-CMAQ and synoptic pressure
836 pattern analysis. Environ. Modell. Softw. 25 (8), 927-934. DOI: 10.1016/j.envsoft.2010.02.004.

837 Wang, G., Cheng, S., Wei, W., Yang, X., Wang, X., Jia, J., Lang, J., and Lv, Z., 2017.
838 Characteristics and emission-reduction measures evaluation of $PM_{2.5}$ during the two major
839 events: APEC and Parade. Sci. Total Environ. 595, 81-92. DOI:
840 10.1016/j.scitotenv.2017.03.231.

841 Wang, G., Zhang, R., Gomez, M.E., Yang, L., Levy Zamora, M., Hu, M., Lin, Y., Peng, J., Guo,
842 S., Meng, J., Li, J., Cheng, C., Hu, T., Ren, Y., Wang, Y., Gao, J., Cao, J., An, Z., Zhou, W.,
843 Li, G., Wang, J., Tian, P., Marrero-Ortiz, W., Secrest, J., Du, Z., Zheng, J., Shang, D., Zeng,
844 L., Shao, M., Wang, W., Huang, Y., Wang, Y., Zhu, Y., Li, Y., Hu, J., Pan, B., Cai, L., Cheng
845 Y., Ji, Y., Zhang, F., Rosenfeld, D., Liss, P.S., Duce, R.A., Kolb, C.E., and Molina, M.J.,
846 2016. Persistent sulfate formation from London fog to Chinese haze. Proc. Natl. Acad. Sci.
847 U.S.A. 113 (48), 13630–13635. DOI: 10.1073/pnas.1616540113.

848 Wang, H., Li, J., Peng, Y., Zhang, M., Che, H., and Zhang, X., 2019. The impacts of the meteorology
849 features on $PM_{2.5}$ levels during a severe haze episode in central-east China. Atmos. Environ.
850 197, 177-189. DOI: 10.1016/j.atmosenv.2018.10.001.

851 Wang, J., Zhang, M., Bai, X., Tan, H., Li, S., Liu, J., Zhang, R., Wolters, M., Qin, X., Zhang, M.,
852 Lin, H., Li, Y., Li, J., and Chen, L., 2017. Large-scale transport of $PM_{2.5}$ in the lower
853 troposphere during winter cold surges in China. Sci. Rep. 7, 13238. DOI: 10.1038/s41598-017-
854 13217-2.

Wang, S., Zhao, M., Wu, Y., Zhou, Y., Lei, Y., He, K., Fu, L., and Hao, J., 2010. Quantifying the air pollutants emission reduction during the 2008 Olympic Games in Beijing. Environ. Sci. Technol. 44 (7), 2490-2496. DOI: 10.1021/es9028167.

Wang, X., Jiang, F., Xu, S., Tian, X., and Yao, D., 2020. Assessment of emergency emission reduction effect during a severe air pollution episode in Yangtze River Delta region. Res. Environ. Sci. accepted. DOI: 10.13198/j.issn.1001-6929.2019.12.12.

Wang, Y., McElroy, M.B., Boersma, K.F., Eskes, H.J., and Veefkind, J.P., 2007. Traffic restrictions associated with the Sino-African summit: Reductions of NO_x detected from space. Geophys. Res. Lett. 2007, 34 (8), 402-420. DOI: 10.1029/2007GL029326.

Wiedinmyer, C., Akagi, S.K., Yokelson, R.J., Emmons, L.K., AlSaadi, J.A., Orlando, J.J., and Soja, A.J., 2011. The Fire Inventory from NCAR (FINN): a high resolution global model to estimate the emissions from open burning. Geosci. Model Dev. 4, 625–641. DOI: 10.5194/gmd-4-625-2011.

Wu, W., Chang, X., Xing, J., Wang, S., and Hao, J., 2017. Assessment of $PM_{2.5}$ pollution mitigation due to emission reduction from main emission sources in the Bejing-Tianjin-Hebei region. Environ. Sci. 38, 867-875. DOI: 10.13227/j.hjkx.201607191.

Zaveri, R.A., Easter, R.C., Fast, J.D., and Peters, L.K., 2008. Model for Simulating Aerosol Interactions and Chemistry (MOSAIC). J. Geophys. Res. Atmos. 113, D13204. DOI: 10.1029/2007JD008782.

Zhang, H., Yuan, H., Liu, X., Yu, J., and Jiao, Y., 2018. Impact of synoptic weather patterns on 24 h-average $PM_{2.5}$ concentrations in the North China Plain during 2013–2017. Sci. Total Environ. 627, 200-210. DOI: 10.1016/j.scitotenv.2018.01.248.

Zhang, H.,Yu, C., Su, L., Wang, Y., and Chen, L., 2017. Analysis on effectiveness of SO_2 and NO_2 emissionreduction in North China Plain by OMI data during the Military Parade 2015. Remot. Sens. Technol. Appl. 32 (4), 734-742. DOI: 10.11873/j.issn.1004-0323.2017.4.0734.

Zhang, J., Xue, H., Deng, Z., Ma, N., Zhao, C., and Zhang, Q., 2014. A comparison of the parameterization schemes of fog visibility using the in-situ measurements in the North China Plain. Atmos. Environ. 92, 44-50. DOI: 10.1016/j.atmosenv.2014.03.068.

Zhang, L., Liu, L.C., Zhao, Y.H., Gong, S.L., Zhang, X.Y., Henze, D.K., Capps, S., Fu, T.M, and Zhang, Q., 2015. Source attribution of particulate matter pollution over North China with the adjoint method. Environ. Res. Lett. 10 (8), 084011, DOI: 10.1088/1748-9326/10/8/084011.

Zhang, L., Shao, J., Lu, X., Zhao, Y., Hu, Y., Henze, D.K., Liao, H., Gong, S., and Zhang, Q., 2016. Sources and processes affecting fine particulate matter pollution over North China: an adjoint analysis of the Beijing APEC period. Environ. Sci. Technol. 50 (16), 8731–8740. DOI: 10.1021/acs.est.6b03010.

Zhang, Q., Ma, Q., Zhao, B., Liu, X., Wang, Y., Jia, B., and Zhang, X., 2018. Winter haze over North China Plain from 2009 to 2016: Influence of emission and meteorology. Environ. Pollut. 242, 1308-1318. DOI: 10.1016/j.envpol.2018.08.019.

Zhang, Q., Streets, D.G., Carmichael, G.R., He, K.B., Huo, H., Kannari, A., Klimont, Z., Park, I.S., Reddy, S., Fu, J.S., Chen, D., Duan, L., Lei, Y., Wang, L.T., and Yao, Z.L., 2009. Asian emissions in 2006 for the NASA INTEX-B mission. Atmos. Chem. Phys. 9, 5131-5153. DOI: 10.5194/acp-9-5131-2009.

Zhang, R., Li, Q., and Zhang, R., 2014. Meteorological conditions for the persistent severe fog and haze event over eastern China in January 2013. Sci. China Earth Sci. 57 (1), 26-35. DOI: 10.1007/s11430-013-4774-3.

Zhao, Y., Liu, Y., Ma, J., Ma, Q., and He, H., 2017. Heterogeneous reaction of SO_2 with soot: The roles of relative humidity and surface composition of soot in surface sulfate formation. Atmos. Environ. 152, 465-476. DOI: 10.1016/j.atmosenv.2017.01.005.

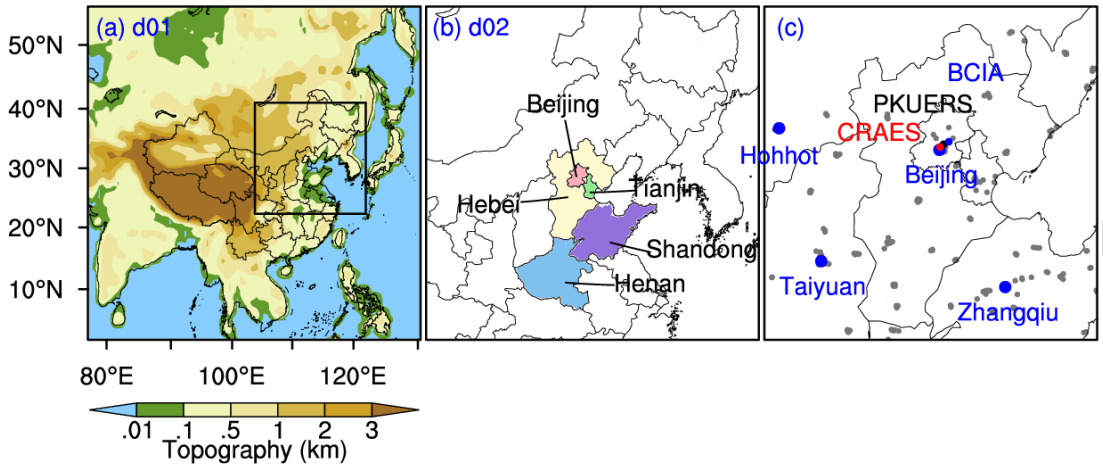

Fig 1. (a) The two nested domains used in our WRF-Chem simulations. The outer domain (d01) is shown with the topography (filled contours). (b) The inner domain (d02) is color-shaded to represent the NCP areas (Beijing, Tianjin, Hebei, Henan, and Shandong), which implemented emission reduction measures during December 6 to 10, 2015. (c) The spatial distribution of meteorology and $PM_{2.5}$ measurement sites used in this study. The blue dots represent the meteorological sites. The black and red dots indicate the PKUERS and CRAES sites with $PM_{2.5}$ concentration and composition measurements. The grey dots indicate other surface sites of $PM_{2.5}$ concentration measurements.

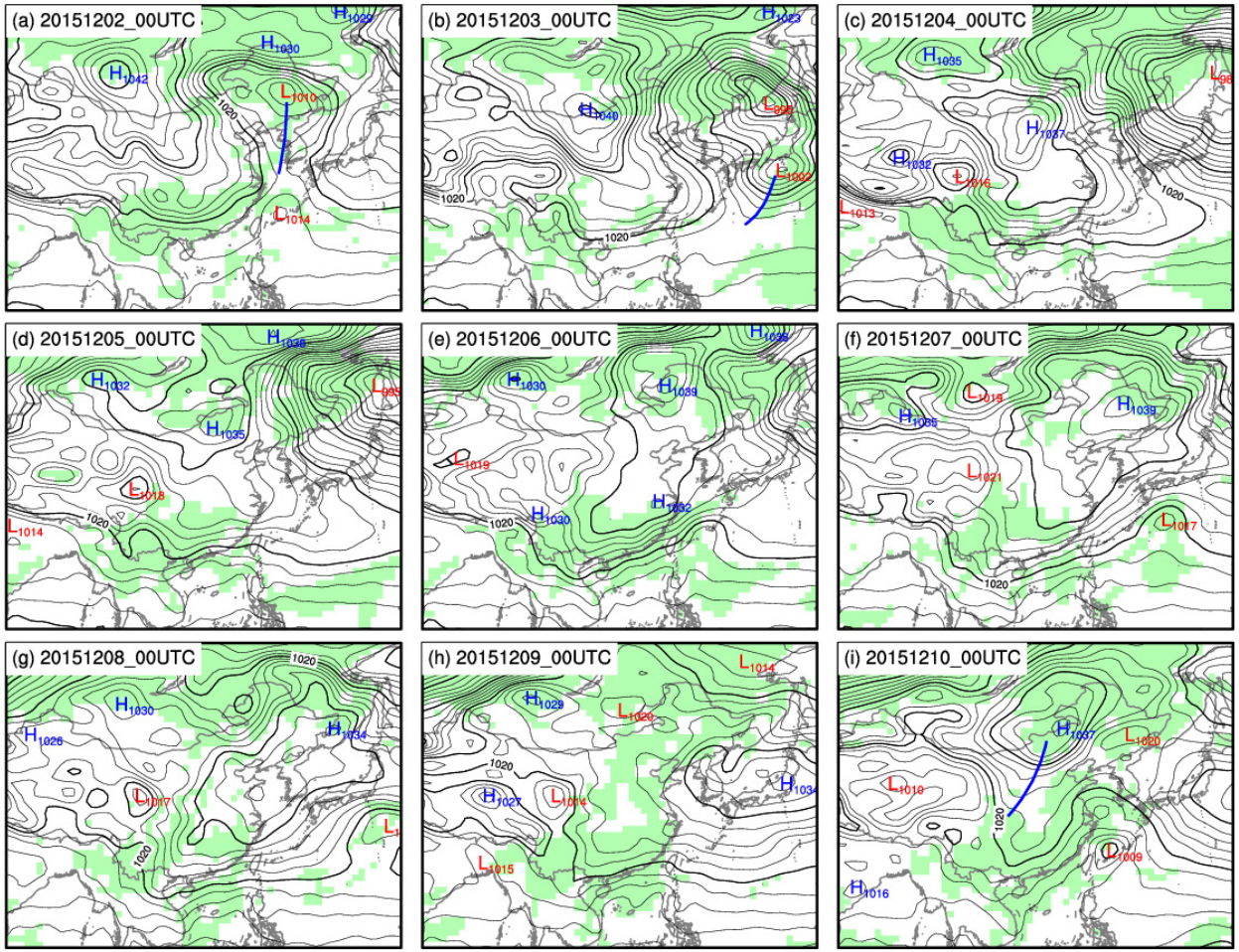

Fig 2. Meteorological conditions over East Asia during December 2 to 10, 2015 from the FNL reanalysis. Black contours indicate sea level pressure (in hPa). Bold blue lines indicate cold fronts. Color-shaded areas indicate surface relative humidity >80%.

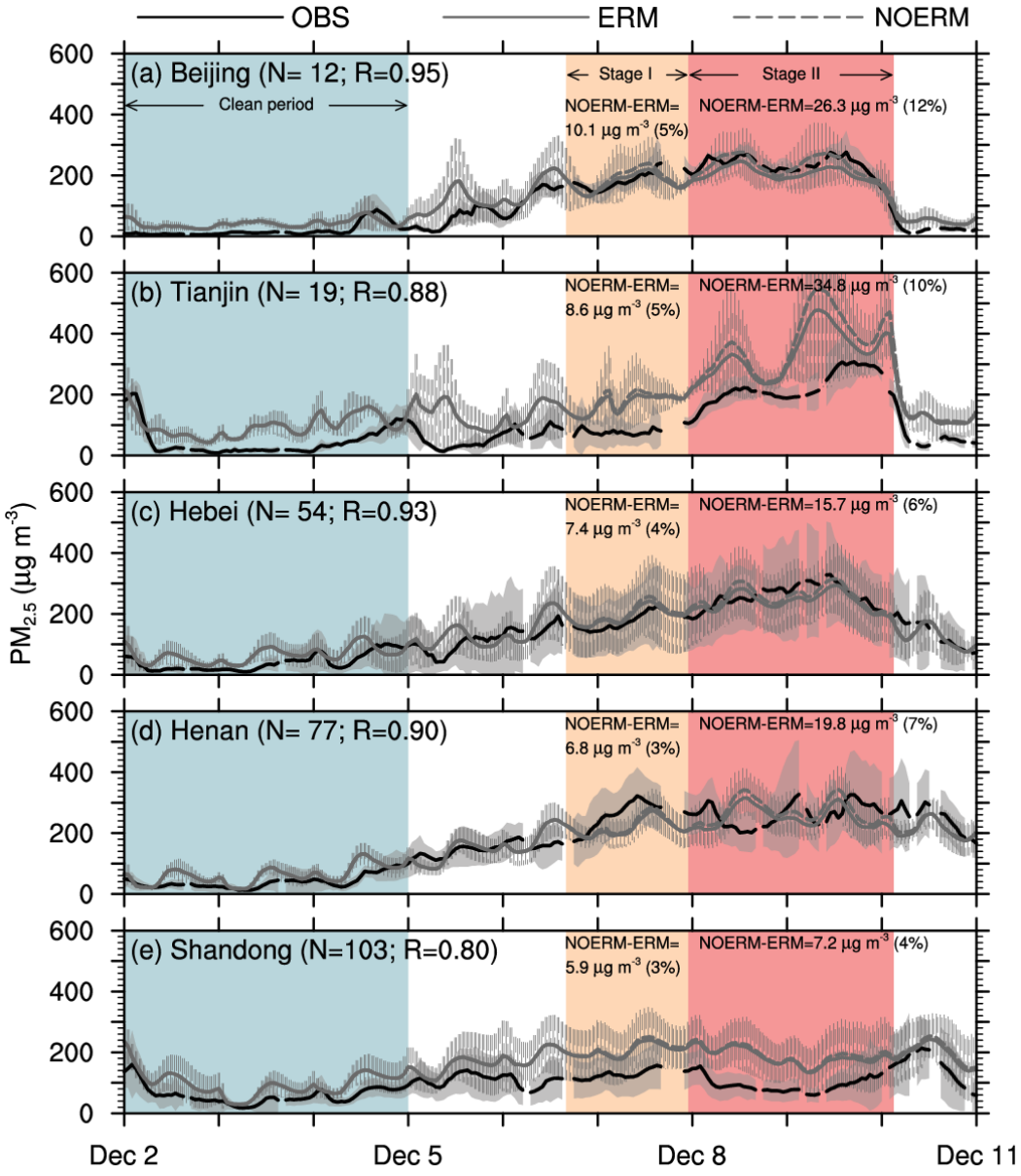

Fig 3. Observed (black solid line) and simulated surface $PM_{2.5}$ concentrations (as average concentrations sampled at surface sites) in (a) Beijing, (b) Tianjin, (c) Hebei, (d) Henan, and (e) Shandong during December 2 to 10, 2015. Simulated concentrations from the NOERM and ERM experiments are shown in dashed grey lines and solid grey lines, respectively. The error bar represents one standard deviation. The site numbers in each province/city (N), the correlation coefficients (R) between the observed concentrations and those simulated in the ERM experiment, simulated concentration differences between the two experiments, as well as the simulated concentration difference percentages between the two experiments are shown inset. The clean period, Stage I, and Stage II are shaded in blue, orange, and red, respectively.

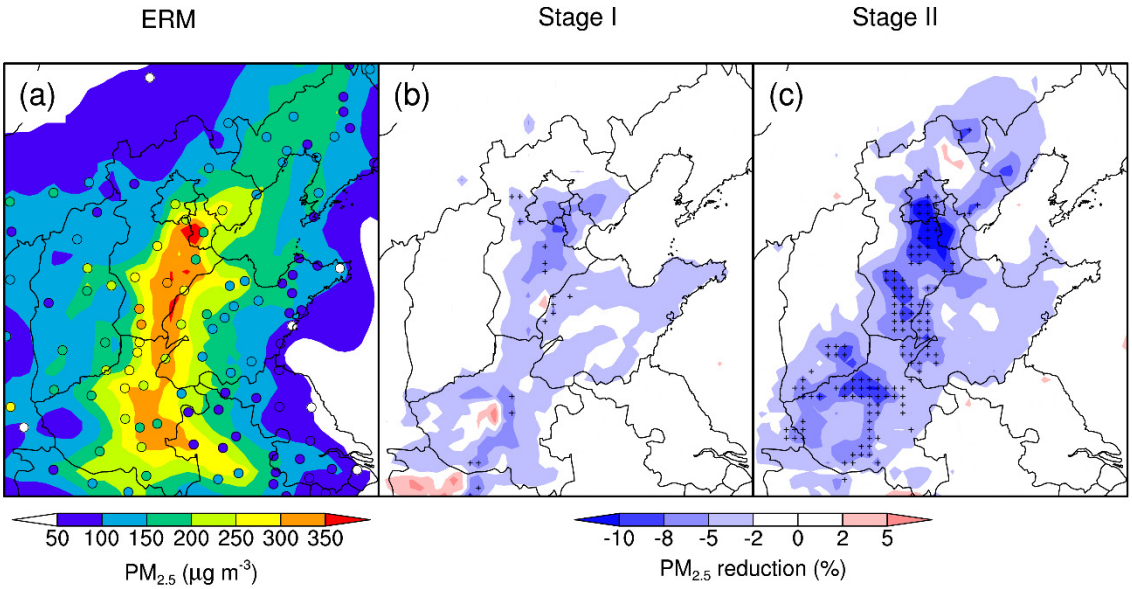

Fig 4. (a) Spatial distribution of the simulated mean surface $PM_{2.5}$ concentrations over NCP during Stage I and Stage II from the ERM experiment, overlaid with the mean concentrations observed at surface sites (filled circles). The percentage of $PM_{2.5}$ concentration changes due to the enforcement of the ERMs during (b) Stage I and (c) Stage II. Grids marked with "+" indicate changes that are statistically significant relative to the hourly concentration variability ($\alpha = 0.05$).

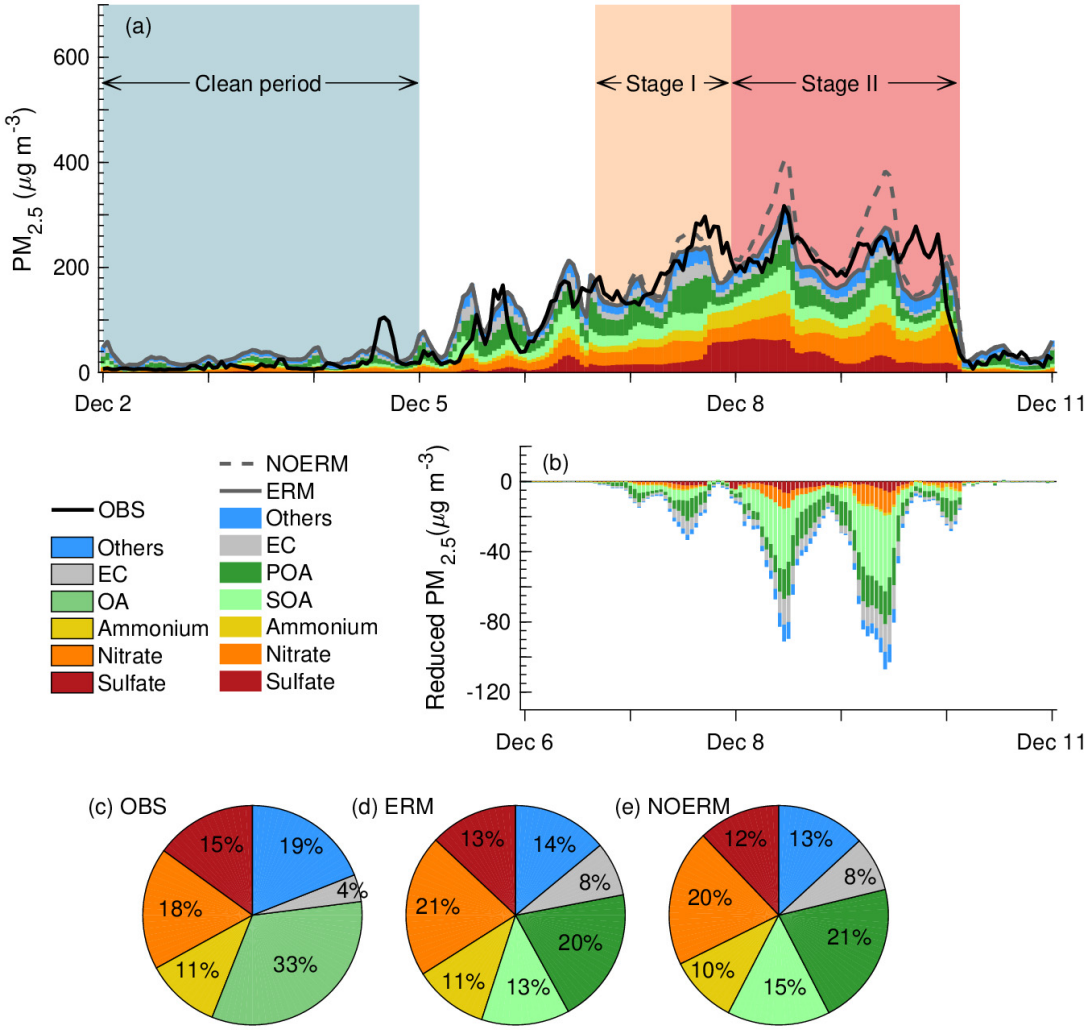

Fig 5. (a) Temporal variations of $PM_{2.5}$ concentrations and components in the ERM experiment (solid grey line and color-filled bars), $PM_{2.5}$ concentrations in the NOERM experiment (dashed grey line), and the observed $PM_{2.5}$ concentration (black line) at the CREAS site in Beijing during December 2 to 10, 2015. (b) The differences in the simulated $PM_{2.5}$ concentrations and compositions at the CREAS site as a result of the ERMs. Also shown are the (c) observed and simulated $PM_{2.5}$ compositions in (d) the ERM and (e) the NOERM experiments during December 6 to 10 at the PKUERS site. Chemical compositions are color-coded. "Others" in the observation indicate non-resolved chemical component. "Others" in the simulation indicate the sum of anthropogenic dust, natural dust, and sea salt.

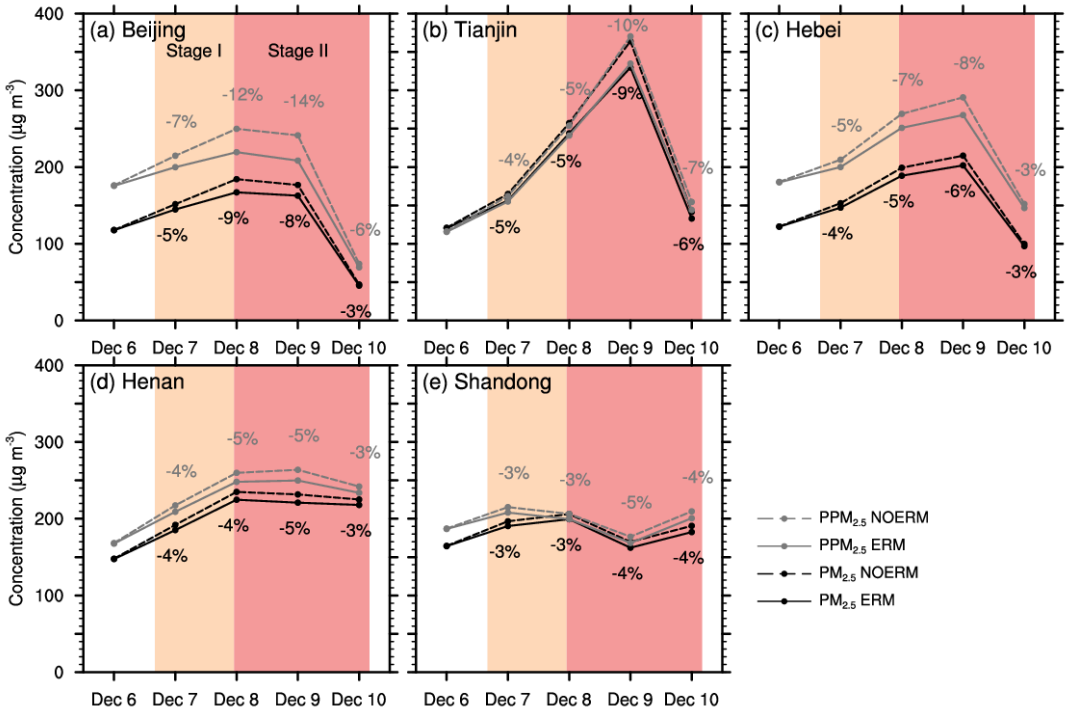

Fig 6. Daily $PM_{2.5}$ and population-weighted $PM_{2.5}$ ($PPM_{2.5}$) variations for (a) Beijing, (b) Tianjin, (c) Hebei, (d) Henan and (e) Shandong during the emission reduction period. The duration of Stage I, and Stage II are shaded in orange and red, respectively.

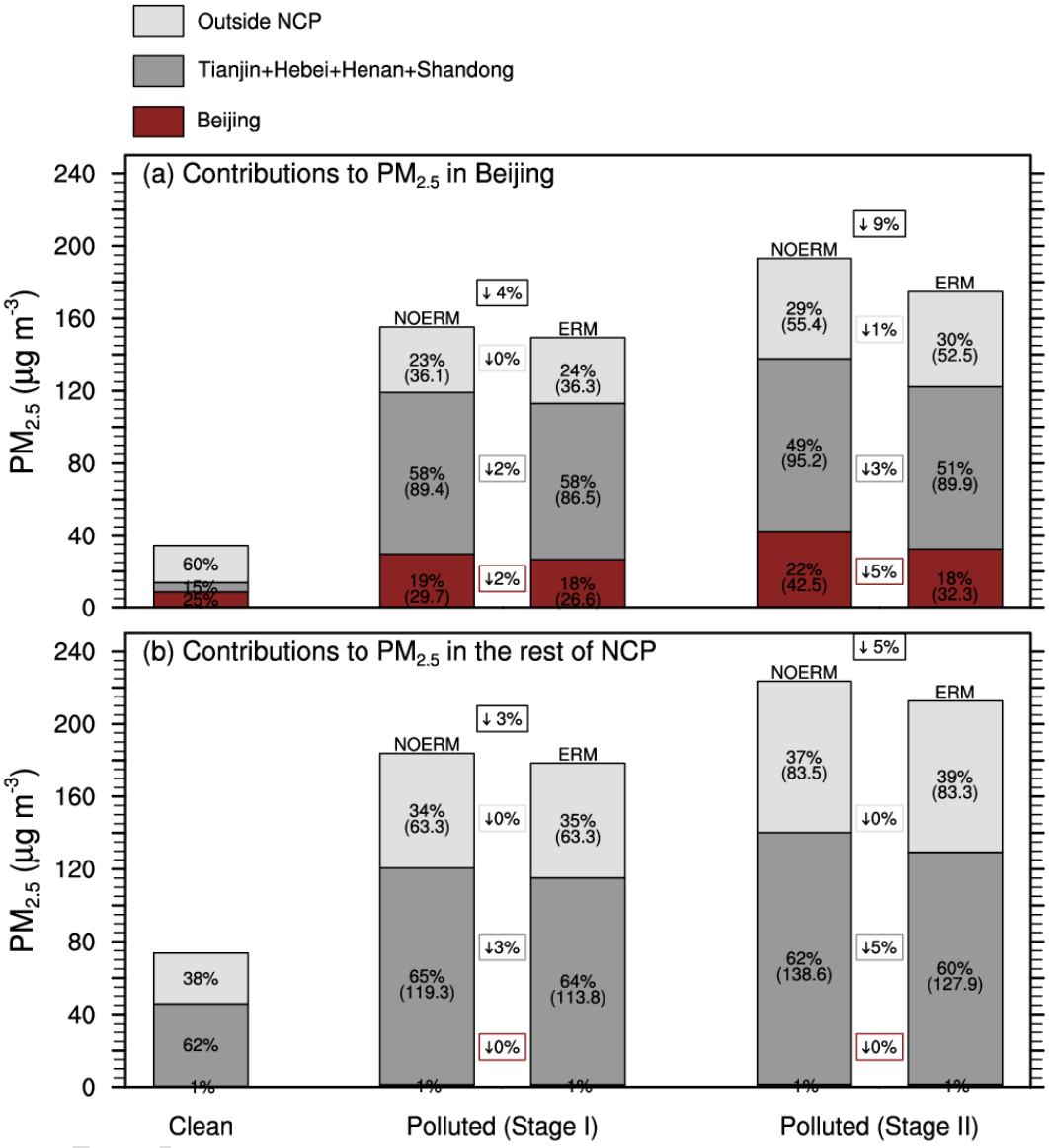

Fig 7. Simulated contributions of local versus regional emissions to $PM_{2.5}$ concentrations in (a) Beijing and (b) the rest of the NCP during the clean period and during the polluted period (Stages I and II). Concentrations and percent contributions from Beijing (red), from the other municipalities within the NCP (dark grey), and from outside the NCP (light grey) are shown inset.

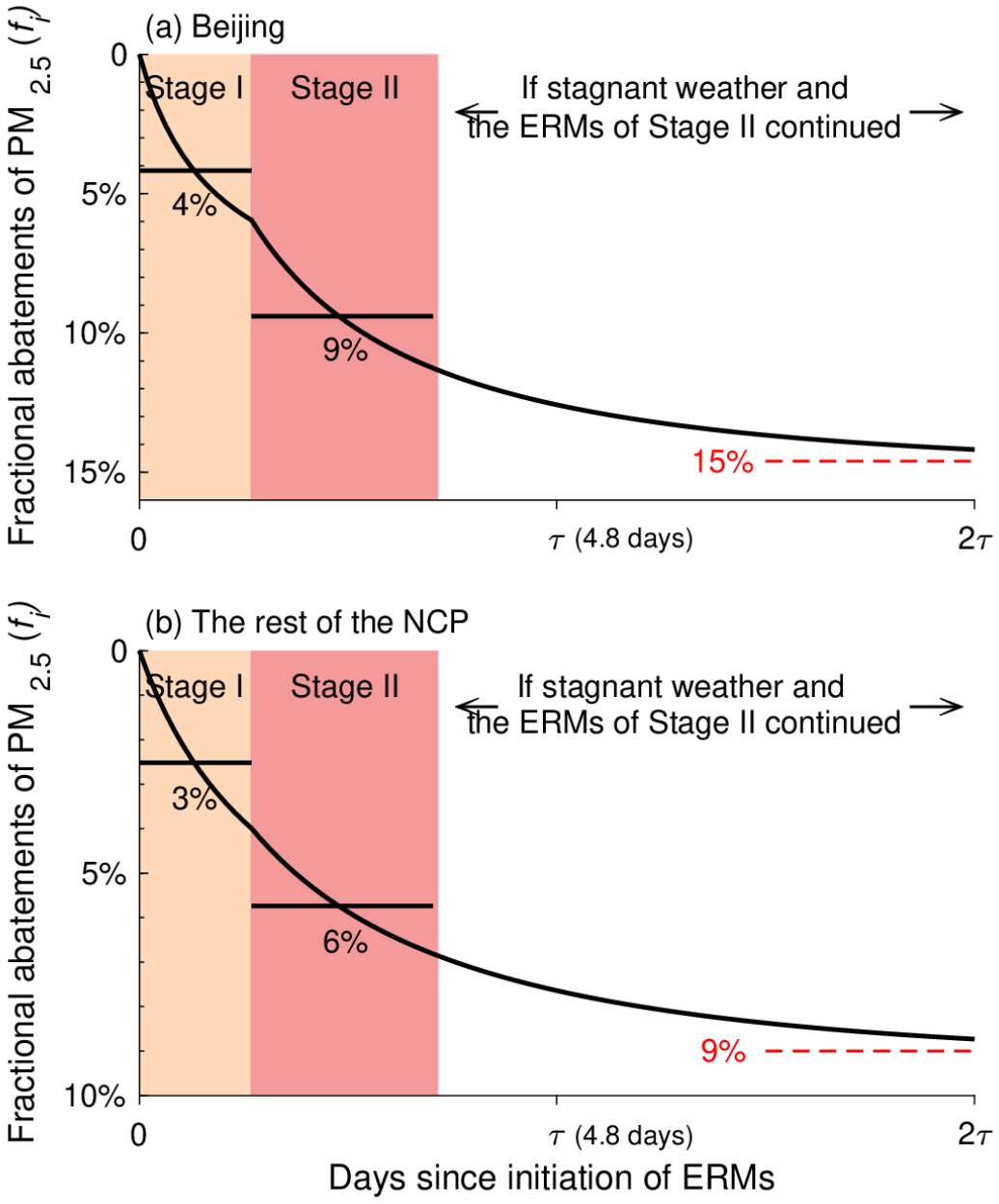

Fig 8. Analytical solutions of the fractional abatements of $PM_{2.5}$ (f_i, black curves) in (a) Beijing and (b) the rest of the NCP as a result of the ERMs implemented, as functions of days since the initiation of ERM enforcement (x-axis). The color blocks indicate the durations of Stages I (orange) and II (red), respectively. The mean analytical fractional abatements of $PM_{2.5}$ during Stages I and II are indicated by the horizontal black lines. The maximum fractional abatements ($f_{max,i}$) of $PM_{2.5}$ are indicated by the red dashed lines.

Table 1 Percent reductions in sectorial anthropogenic emissions associated with the various alert levels issued by the cities and provinces in the NCP during December 6 to 10, 2015

City/Province	Sector	Percentage of emission reduction		
		Yellow alert	Orange alert	Red alert
Beijing	Power generation	- [a]	0 [b]	0
	Industry	-	-15%	-50%
	Residential activities	-	-10%	-30%
	Transportation	-	-30%	-42%
Tianjin	Power generation	0	0	-
	Industry	-20%	-30%	-
	Residential activities	-10%	-10%	-
	Transportation	0	0	-
Hebei	Power generation	0	0	-
	Industry	-15%	-30%	-
	Residential activities	-10%	-10%	-
	Transportation	-20%	-20%	-
Henan	Power generation	-	0	-
	Industry	-	-30%	-
	Residential activities	-	-10%	-
	Transportation	-	-20%	-
Shandong	Power generation	0	-	-
	Industry	-10%	-	-
	Residential activities	-10%	-	-
	Transportation	-10%	-	-

[a] '-' indicates that the alert level was not issued.

[b] '0' indicates that no emission reductions associated with the sector at the issued alert level.

Table 2 Pollutant emissions from the cities and provinces in the NCP and the associated percent reductions during Stages I [a] and II [b]

	Base emissions / alert levels	EC	Primary OC [c]	Other primary $PM_{2.5}$	VOCs	SO_2	NOx	NH_3	CO
Beijing	Base (Mg)	23	62	71	1299	125	699	61	4362
	Stage I reduction	-13%	-11%	-12%	-15%	-12%	-18%	-4%	-14%
	Stage II reduction	-34%	-31%	-35%	-48%	-34%	-38%	-9%	-34%
Tianjin	Base (Mg)	49	82	118	1818	503	1181	96	6349
	Stage I reduction	-11%	-11%	-13%	-18%	-17%	-14%	-1%	-12%
	Stage II reduction	-14%	-12%	-16%	-27%	-24%	-21%	-2%	-16%
Hebei	Base (Mg)	387	686	697	4929	2823	4963	1212	45560
	Stage I reduction	-12%	-11%	-12%	-14%	-13%	-14%	-1%	-12%
	Stage II reduction	-16%	-13%	-18%	-24%	-22%	-23%	-2%	-18%
Henan	Base (Mg)	330	599	691	5110	1918	3920	2176	32374
	Stages I and II reduction	-17%	-13%	-19%	-24%	-20%	-20%	-2%	-17%
Shandong	Base (Mg)	413	804	1127	8357	42218	6588	1689	45260
	Stages I and II reduction	-10%	-10%	-9%	-10%	-8%	-8%	-1%	-10%

[a] Stage I referred to 16:00 UTC of December 6 to 23:00 UTC of December 7, during which the orange alert was in effect in Beijing

[b] Stage II referred to 23:00 UTC of December 7 to 04:00 UTC of December 10, during which the red alert was in effect in Beijing

[c] Input into WRF-Chem as organic carbon

Table 3 Design of the sensitivity experiments used in this study

Experiments	Emission scenario
NOERM	Chinese anthropogenic emissions taken from the MEIC inventory with no reduction
ERM (control)	Same as NOERM, except anthropogenic emissions reduced in Beijing, Tianjin, Hebei, Henan, and Shandong during December 6 to 10 (Stages I and II) as a result of the enforcement of the ERMs (Table 2)
ERM_NOBJ	Same as ERM except no anthropogenic emissions in Beijing
ERM_NOOTH	Same as ERM except no anthropogenic emissions in Tianjin, Hebei, Henan, and Shandong
NOERM_NOBJ	Same as NOERM except no anthropogenic emissions in Beijing
NOERM_NOOTH	Same as NOERM except no anthropogenic emissions in Tianjin, Hebei, Henan, and Shandong.